JCB Journal of Cell Biology

TOOLS

TanGIBLE: A selective probe for evaluating hydrophobicity-exposed defective proteins in live cells

Yasuyuki Iwasa[1*], Sohtaroh Miyata[1*], Takuya Tomita[2], Naoto Yokota[1], Maho Miyauchi[1], Ruka Mori[1], Shin Matsushita[1], Rigel Suzuki[1], Yasushi Saeki[2], and Hiroyuki Kawahara[1]

The accumulation of defective polypeptides in cells is a major cause of various diseases. However, probing defective proteins is difficult because no currently available method can retrieve unstable defective translational products in a soluble state. To overcome this issue, there is a need for a molecular device specific to structurally defective polypeptides. In this study, we developed an artificial protein architecture comprising tandemly aligned BAG6 Domain I, a minimum substrate recognition platform responsible for protein quality control. This tandem-aligned entity shows enhanced affinity not only for model defective polypeptides but also for endogenous polyubiquitinated proteins, which are sensitive to translational inhibition. Mass-spectrometry analysis with this probe enabled the identification of endogenous defective proteins, including orphaned subunits derived from multiprotein complexes and misassembled transmembrane proteins. This probe is also useful for the real-time visualization of protein foci derived from defective polypeptides in stressed cells. Therefore, this "new molecular trap" is a versatile tool for evaluating currently "invisible" pools of defective polypeptides as tangible entities.

Introduction

The accumulation of defective polypeptides in cells contributes to many pathological conditions. For example, the onset of type 1 diabetes (Skowera et al., 2008; Liu et al., 2012; Guo et al., 2014; Braunstein et al., 2015; Ciechanover and Kwon, 2015) and neurodegenerative disorders (Ross and Poirier, 2004; Rane et al., 2008, 2010) is likely stimulated by cellular stresses induced by defective proteins. However, the extremely high diversity of defective translational products and their instability in living cells are major obstacles in identifying endogenous defective polypeptides. At present, the only available method for retrieving defective proteins from stressed cells is differential size exclusion (e.g., centrifugation), in which proteins are retrieved as insoluble aggregates (Koplin et al., 2010; Geladaki et al., 2019; Brennan et al., 2019). However, this approach is not suitable for evaluating the presence of cytotoxic oligomers prior to their aggregation (Escusa-Toret et al., 2013). Furthermore, the components of phase-separated structures, such as stress granules (SGs), are not significantly enriched in aggregates purified by centrifugation (Koplin et al., 2010; Brennan et al., 2019), suggesting that defective proteins that are not included in sedimentable aggregates are less likely to be identified using conventional methods. In addition, proteins found in aggregates generally have low intrinsic turnover rates (Brennan et al., 2019), whereas a non-negligible portion of defective proteins is rapidly degraded (Dephoure et al., 2014). Overcoming these issues requires the development of methods that can retrieve defective proteins in the liquid phase, although this is considered a challenging task.

Exposure of hydrophobic amino acids to the aqueous environment is a common characteristic of structurally defective translational products. Indeed, hydrophobic side chains that are buried in natively folded proteins tend to be exposed following misfolding and act as a signal for degradation in the cytosol (Gilon et al., 1998; Huang et al., 2011; Metzger et al., 2008; Suzuki and Kawahara, 2016). These defective polypeptides are degraded immediately after synthesis, and their degradation products are a major source of antigenic peptides for major histocompatibility complex (MHC) class I–restricted antigen presentation (Schubert et al., 2000; Reits et al., 2000; Khan et al., 2001; Qian et al., 2006; Yewdell et al., 2003, 2011). Defective polypeptides can be stabilized by treatment with proteasome inhibitors and accumulate as polyubiquitinated species (Goldberg, 2012).

[1]Department of Biological Sciences, Laboratory of Cell Biology and Biochemistry, Tokyo Metropolitan University, Tokyo, Japan; [2]Department of Protein Metabolism, Institute of Medical Science, The University of Tokyo, Tokyo, Japan.

*Y. Iwasa and S. Miyata contributed equally to this paper. Correspondence to Hiroyuki Kawahara: hkawa@tmu.ac.jp.

However, polyubiquitinated proteins in proteasome-suppressed cells comprise not only defective proteins but also "structurally normal" proteasomal substrates. These intrinsically short-lived normal proteins are difficult to distinguish from "minor" aberrant proteins. Therefore, it is imperative to develop a specific probe that allows the retrieval of hydrophobicity-exposed defective proteins from cells under native conditions. Here, we describe the invention of such a probe, which has a tandem-repeated architecture based on the hydrophobicity recognition domains of the BAG6 protein.

BAG6 (alternatively called BAT3 or Scythe) is an MHC-encoded multidomain protein with a ubiquitin-like (UBL) sequence (Banerji et al., 1990; Kawahara et al., 2013; Lee and Ye, 2013) that binds to hydrophobic targets, such as defective translation products derived from abnormally spliced transcripts (Kikukawa et al., 2005), newly synthesized defective polypeptides such as mislocalized proteins (Minami et al., 2010; Hessa et al., 2011; Wang et al., 2011; Rodrigo-Brenni et al., 2014; Wunderley et al., 2014; Kawahara et al., 2013; Lee and Ye, 2013; Suzuki and Kawahara, 2016), and ERAD substrates (Xu et al., 2013; Payapilly and High, 2014). BAG6 exhibits affinity for the hydrophobic side chains of client proteins (Kikukawa et al., 2005; Minami et al., 2007, 2010; Wang et al., 2011; Hessa et al., 2011; Payapilly and High, 2014; Tanaka et al., 2016; Takahashi et al., 2019) and captures newly synthesized defective proteins through their exposed hydrophobicity concomitant with or after their release from the ribosome (Minami et al., 2010; Hessa et al., 2011; Wang et al., 2011; Xu et al., 2013; Guna and Hegde, 2018). Recent genome-wide analyses have revealed that the hydrophobic C-termini of readthrough products with translated 3′-UTRs are recognized by BAG6 for proteasomal degradation (Müller et al., 2023). BAG6 is also critical for the surveillance of hydrophobic noncoding genome translation models (Kesner et al., 2023). Similarly, CRISPR-mediated screens identified BAG6 as a primary factor for the degradation of a variety of short-hydrophobicity-exposed degron models (Zhang et al., 2023). Therefore, the substrate recognition domain of BAG6 provides a promising element for probing a wide variety of hydrophobicity-exposed defective polypeptides.

BAG6 is a multidomain protein that supports the recruitment of various hydrophobic substrates (Kikukawa et al., 2005; Minami et al., 2010; Kawahara et al., 2013; Tanaka et al., 2016). The C-terminal BAGS/Mock BAG domain is required for tail-anchored protein biogenesis (Mock et al., 2015; Kuwabara et al., 2015), whereas the N-terminal region of BAG6 is critical for the proteasome-mediated degradation of defective proteins (Fig. 1 A). Indeed, deletion of the N-terminal 465 residues of full-length (FL) BAG6 (Δ1–465 BAG6) completely abolishes its recognition of hydrophobicity-exposed polyubiquitinated proteins (Kikukawa et al., 2005; Minami et al., 2010; Tanaka et al., 2016), suggesting that this region is essential for recognizing defective proteins (Minami et al., 2010; Rodrigo-Brenni et al., 2014; Tanaka et al., 2016).

Previous studies identified two functionally redundant sequences within the N-terminal 465 residues of human BAG6: Domain I (residues 1–215) and Domain II (residues 216–465) (Fig. S1 A) (Kikukawa et al., 2005; Kawahara et al., 2013; Tanaka et al., 2016). These segments can redundantly and directly capture the exposed hydrophobicities of the client proteins (Kikukawa et al., 2005; Tanaka et al., 2016). Domain I can be further subdivided into two evolutionarily conserved and structurally ordered islands: UBL (residues 17–92 of human BAG6) and BUILD (residues 126–184) domains (Tanaka et al., 2016) (Fig. S1 A). Neither the UBL nor BUILD domains are sufficient for hydrophobic binding with substrates but rather collaborate to form a functional substrate recognition segment (Kikukawa et al., 2005; Tanaka et al., 2016). Thus, Domain I is a minimum platform that participates in discriminating substrates with exposed hydrophobic residues, which act as a degradation signal.

Although Domain I is potentially useful for detecting defective proteins, its ability to retrieve client polypeptides is low compared with the case in the N-terminal 465 residue fragment of BAG6 (a fragment comprising tandemly aligned Domains I and II). Domain II includes the "domain of unknown function (DUF)" 3538 (Fig. S1 A) (Xu et al., 2013; Kawahara et al., 2013; Tanaka et al., 2016). Domain II exhibits a high affinity comparable with that of Domain I for the exposed hydrophobicity of misfolded protein models (Kikukawa et al., 2005; Xu et al., 2013), while the Domain II fragment is highly aggregation-prone and unstable, making this fragment unsuitable as a probe. Fortunately, the Domain I fragment is highly soluble and stable both in vivo and in vitro (Minami et al., 2010; Tanaka et al., 2016), making Domain I an attractive device for the recognition of defective proteins. We therefore constructed an artificial protein architecture based on tandemly aligned Domain I fragments. In this study, we provide evidence that this tandemly aligned construct shows markedly improved affinity for model defective substrates. Furthermore, mass-spectrometry (MS) analysis with this probe enabled the identification of endogenous orphaned subunits derived from multiprotein complexes and of misassembled transmembrane proteins, providing an effective way to identify uncharacterized defective species. This probe is also suitable for the real-time visualization of cytoplasmic foci formation processes stimulated by various proteotoxic stresses in a single living cell. Therefore, this "new molecular trap" is a versatile tool for isolating, visualizing, and quantifying endogenous hydrophobicity-exposed polypeptides and should facilitate a better understanding of the enigmatic pool of defective proteins induced by various physiological and pathological conditions.

Results

Architecture of the tandem UBL-BUILD entity

To establish a potentially useful molecular probe for hydrophobicity-exposed defective proteins, we focused on the BAG6 Domain I, a minimum substrate-recognizing segment derived from the BAG6 N-terminus (Fig. 1A and Fig. S1 A) (Kikukawa et al., 2005; Minami et al., 2010; Kawahara et al., 2013; Tanaka et al., 2016). We fused two identical fragments of Domain I through a flexible glycine linker and designated this artificial fragment as "Tandem BAG6 domain I BUILD linked entity" (TanGIBLE). This architecture consists of four tandemly aligned conserved sequences, two UBL domains (Fig. 1 B, shown in violet), and two

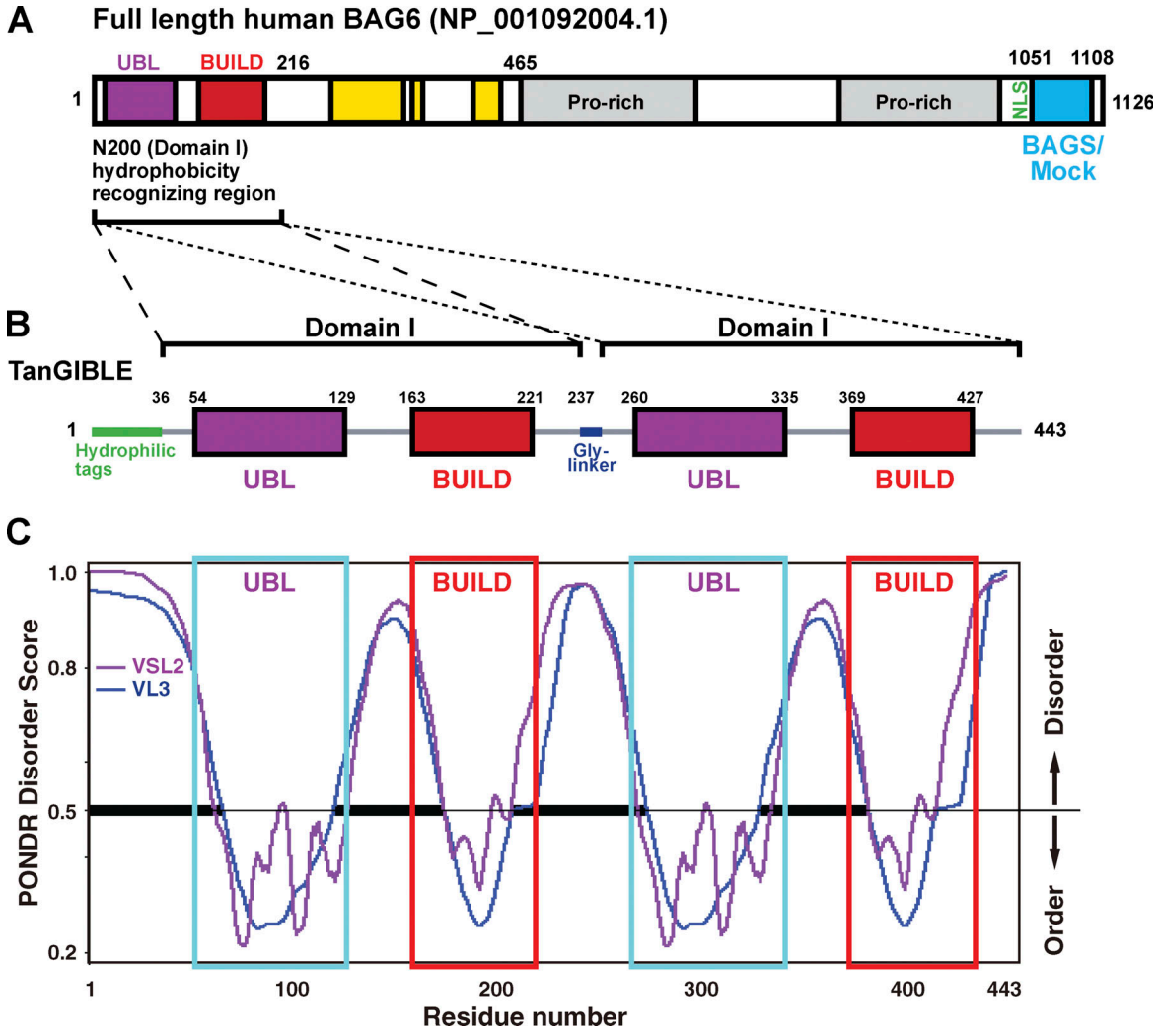

Figure 1. **Schematics of the domain structure of BAG6 and its derivative architecture designed in this study. (A)** Schematic of the human FL form of BAG6 protein (NP_001092004.1). The positions of Domains I (N200) and other domains are indicated. Numbers denote the corresponding amino acid positions. **(B)** Schematic of the domain structure of the TanGIBLE developed in this study. Domain I is composed of two highly conserved regions, UBL (indicated by violet squares) and BUILD (indicated by red squares). Note that TanGIBLE consists of two Domain I units tandemly connected with a glycine (Gly) linker. N-terminal hydrophilic tags are shown in green. **(C)** TanGIBLE is composed of four tandemly aligned ordered domains. The amino acid sequence of TanGIBLE was analyzed using the disorder/order structure prediction programs PONDR. Stretches corresponding to the UBL sequence are indicated with a blue box and those corresponding to the BUILD sequence are indicated with a red box. The results from two different predictor packages, VSL2 (violet line) and VL3 (blue line), are shown.

BUILD domains (Fig. 1 B, shown in red). To improve handling efficiency, we fused hydrophilic tags, such as T7, Flag, and fluorescent proteins, at the N- (or C-) terminus of this construct (Fig. 1 B, shown in green). Analysis of the amino acid sequence of TanGIBLE using the secondary structure prediction program PONDR (https://www.pondr.com) provided low disorder scores for the UBL and BUILD sequences (Fig. 1 C, blue boxes for UBL and red boxes for BUILD regions) and highly disordered intervening sequences. These results suggest that TanGIBLE comprises four tandemly aligned structured domains.

TanGIBLE shows increased affinity with a model defective protein

Most transmembrane domain (TMD) proteins and secretory proteins are translocated into the lumen of the endoplasmic reticulum (ER) via a signal sequence (SS)–mediated co-translational process (Walter and Johnson, 1994; Keenan et al., 2001). However, a non-negligible portion of SRP-client models failed to translocate correctly into the lumen of the ER (Levine et al., 2005; Guna and Hegde, 2018), resulting in the production of mislocalized polypeptides (MLPs) in the cytosol. Such newly synthesized defective proteins tend to expose highly hydrophobic orphan domains to the aqueous cytosol (Guna and Hegde, 2018) and are thus immediately targeted to the ubiquitin-mediated protein degradation pathway (Hessa et al., 2011; Suzuki and Kawahara, 2016; Yamamoto et al., 2017).

The IL-2 receptor α subunit (IL-2Rα) is a single-pass TM protein that contains a typical SS for ER insertion at its N-terminus and a TMD at its C-terminus (Fig. 2 A, FL). Deleting the SS from IL-2Rα (Fig. 2 A, ΔSS) makes this protein inaccessible

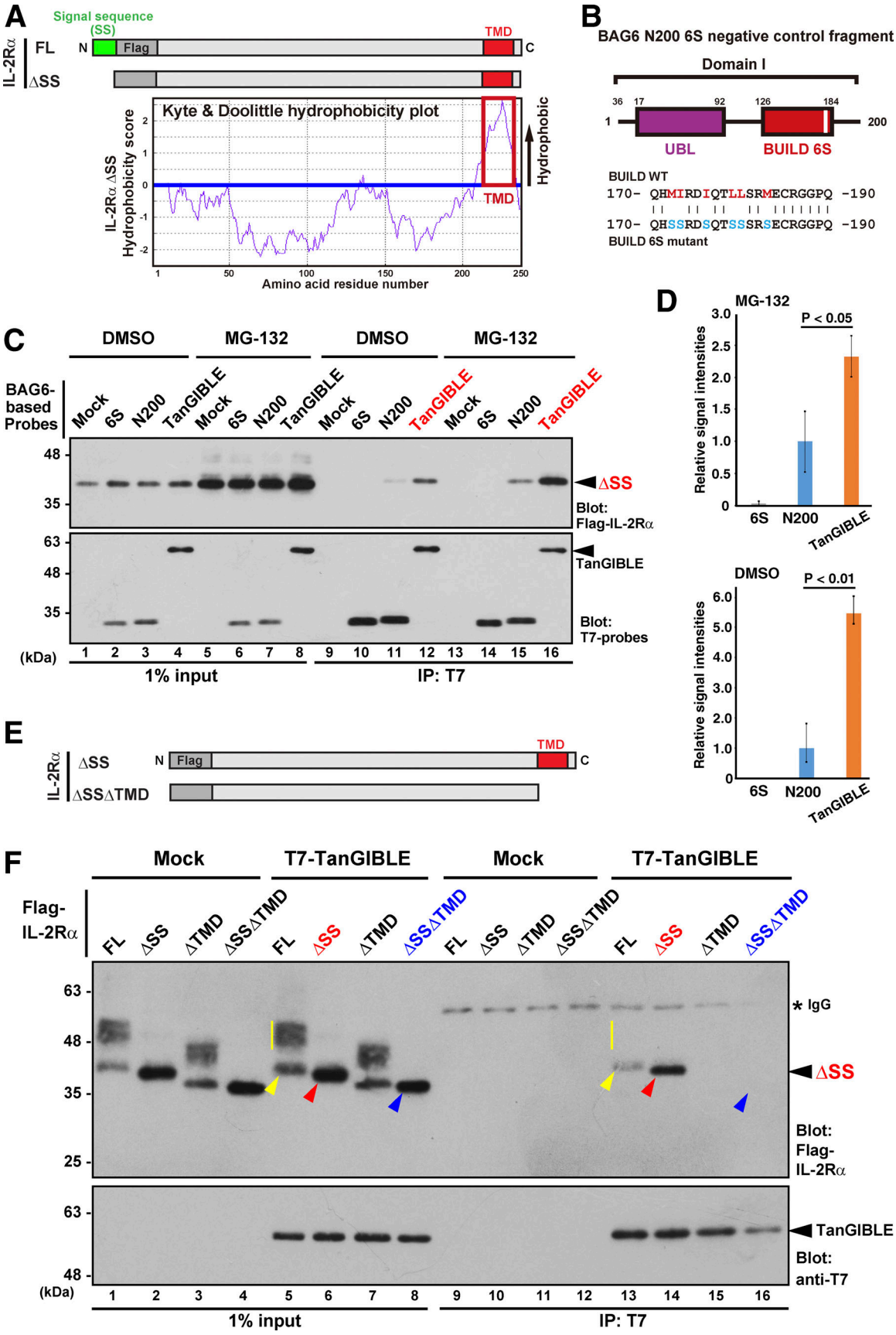

Figure 2. **Detection of mislocalized TMD protein using TanGIBLE. (A and E)** Schematic of the Flag-tagged IL-2Rα protein and its derivatives used in this study. The SS is indicated in green, while the TMD is indicated in red (upper panel). Kyte-Doolittle hydrophobicity plots of IL-2Rα ΔSS protein (A, lower panel).

The single hydrophobicity peak at the C-terminus of IL-2Rα ΔSS corresponds exactly to the TMD (red box). The numbers on the horizontal axis denote the corresponding amino acid positions in this protein. FL: full-length. **(B)** Six conserved hydrophobic residues in the tail of the BUILD domain of human BAG6 (Met^{172}, Ile^{173}, Ile^{176}, Leu^{179}, Leu^{180}, and Met^{183}) are indicated with red characters. These are essential for the recognition of CL1 degron hydrophobicity by BAG6 Domain I (Tanaka et al., 2016). Substitution of these hydrophobic residues with hydrophilic serine (designated N200-6S fragment, indicated with blue characters) abolished its binding ability with model defective polypeptides. This mutant protein was utilized as one of the negative controls. **(C)** Co-immunoprecipitation (IP) of Flag-IL-2Rα ΔSS with T7-tagged TanGIBLE, N200-6S, and N200 fragments in the presence or absence of MG-132. 24 h after transfection with expression plasmids, HeLa cells were treated with 10 μM MG-132 or vehicle (DMSO) for 4 h. The precipitates formed with anti-T7 agarose were subjected to western blot analysis with anti-Flag and anti-T7 antibodies. **(D)** Quantification of IL-2Rα ΔSS co-immunoprecipitated with TanGIBLE in panel B. The intensity of the co-precipitated IL-2Rα ΔSS signals with the BAG6 N200 fragment was defined as the standard (as 1.0), and the relative values of IL-2Rα ΔSS co-precipitates are indicated. The data represent the mean ± SD calculated from three biologically independent experiments (n = 3). P values were calculated using Student's t test between N200 and TanGIBLE. **(F)** TanGIBLE recognizes a mislocalized transmembrane protein through its unembedded TMD. A series of Flag-tagged IL-2Rα proteins were expressed in HeLa cells with T7-tagged TanGIBLE in the presence of 10 μM MG-132, and T7 immunoprecipitates were blotted with anti-Flag antibody. The smear signals (indicated with a yellow line) in the input lane represent glycosylated (and thus successfully incorporated into the ER lumen) forms of IL-2Rα. Mislocalized forms of IL-2Rα ΔSS and FL, co-immunoprecipitated with TanGIBLE, are indicated with red and yellow arrowheads, respectively. Blue arrowheads indicate mislocalized species with a deleted TMD. Source data are available for this figure: SourceData F2.

to the ER and destabilizes it, making the protein for ubiquitin-dependent degradation as a typical MLP (Huang et al., 2011; Suzuki and Kawahara, 2016). The exposed TMD of misassembled IL-2Rα in the cytosol functions as a major degradation signal for proteasomal destruction (Huang et al., 2011; Suzuki and Kawahara, 2016). Therefore, IL-2Rα ΔSS provides an ideal model for evaluating the ability of the probe to recognize newly synthesized (and rapidly degraded) mislocalized TM proteins in the cytosol.

To validate the ability of our experimental system to retrieve defective polypeptides, we showed that the BAG6 N-terminal 200 residue Domain I fragment (designated as N200) co-immunoprecipitates with IL-2Rα ΔSS from cell extracts in the presence of the protease inhibitor MG-132 (Fig. 2 C, lane 15). In contrast, N200-6S (a mutated N200 fragment whose critical hydrophobic residues are substituted with serine, Fig. 2 B) (Tanaka et al., 2016) shows little affinity for IL-2Rα ΔSS, even in the presence of MG-132 (Fig. 2 C, lane 14). We found that TanGIBLE co-precipitated with IL-2Rα ΔSS more than with BAG6 N200 (Fig. 2 C, compare lanes 15 and 16; see also Fig. S1 B). Quantification of the signal intensity of IL-2Rα ΔSS suggested that, in the presence of MG-132, TanGIBLE co-precipitated 2.4-fold more IL-2Rα ΔSS compared with BAG6 N200 fragment at a statistically significant level (Fig. 2 D, upper panel). Furthermore, TanGIBLE retrieved 5.6-fold more IL-2Rα ΔSS than BAG6 N200 in the absence of MG-132 (Fig. 2 D, lower panel). TanGIBLE co-immunoprecipitated IL-2Rα ΔSS more than BAG6 N465, a fragment with tandemly aligned Domains I and II (Fig. S1, C and D). These observations suggest that TanGIBLE has an enhanced affinity for IL-2Rα ΔSS, a model mislocalized transmembrane protein.

Cytosol-exposed hydrophobicity of MLP is critical for recognition by TanGIBLE

The specificity of TanGIBLE toward potential client proteins is critical for utilizing this artificial protein as a probe for defective proteins. We, therefore, examined how TanGIBLE recognizes the misassembled TM protein IL-2Rα as a model example. For FL IL-2Rα, most of the protein was detected as smears on western blot analysis due to glycosyl modification (Fig. 2 F, yellow lines in input lane 5), suggesting that most of the protein was successfully assembled into the ER lumen (Suzuki and Kawahara, 2016). In contrast, a portion of IL-2Rα FL was detected as a non-glycosylated (and thus ER-incorporation-failed) defective species (Fig. 2 F, yellow arrowhead in lane 5) (Ma and Lindquist, 2001; Chakrabarti et al., 2011; Rane et al., 2004). Importantly, TanGIBLE selectively retrieved the non-glycosylated form of IL-2Rα FL (Fig. 2 F, yellow arrowhead in IP lane 13) but hardly interacted with the major glycosylated (successfully synthesized) species of IL-2Rα FL (Fig. 2 F, yellow line in IP lane 13). These observations clearly indicate that TanGIBLE has a strong preference for misassembled TM protein models but does not recognize successfully assembled membrane proteins with a membrane-embedded TMD.

We next asked whether the unembedded TMD of mislocalized IL-2Rα ΔSS is critical for recognition by TanGIBLE. We thus prepared a TMD-deleted mutant of IL-2Rα ΔSS (Fig. 2 E, ΔSSΔTMD). Although TanGIBLE co-precipitated with IL-2Rα ΔSS as noted above (Fig. 2 F, lane 14, red arrowheads), it scarcely precipitated the TMD-deleted mutant (Fig. 2 F, lane 16, ΔSSΔTMD, blue arrowhead). Given that the TMD is the only hydrophobic segment in IL-2Rα ΔSS (Fig. 2 A, hydrophobicity plot), these results suggest that the orphaned hydrophobic domain of IL-2Rα ΔSS is indispensable for recognition by TanGIBLE.

To elucidate whether a shorter and less hydrophobic stretch can also be targeted by TanGIBLE, we examined the affinity of TanGIBLE with another metastable protein model, CL1-fused luciferase (Fig. S2 A), a moderately hydrophobicity-exposed non-TMD polypeptide (Gilon et al., 1998; Metzger et al., 2008; Tanaka et al., 2016). Similar to IL-2Rα ΔSS, TanGIBLE co-precipitated more CL1-fused luciferase than the BAG6 N200 fragment (Fig. S2, B and C). Thus, we concluded that cytosol-exposed hydrophobic segments, not only TMD but also short stretches of hydrophobic residues, are targets for recognition by TanGIBLE.

An insulin mutant associated with type I diabetes is recognized by TanGIBLE

Given that TanGIBLE retrieved artificial defective protein models (Fig. 2 and Fig. S2, A–C), we were curious whether TanGIBLE can also recognize "real" defective proteins involved

in the etiology of human diseases. Several heterozygous point mutations within the SS of insulin have been identified in pedigrees with type I diabetes (Støy et al., 2007; Polak et al., 2008). These include the R6C mutant, which contains an Arg^{6} to Cys^{6} substitution (Fig. S2 D) (Edghill et al., 2008). Although such heterozygous patients possess an intact insulin gene on the other chromosome, they nevertheless develop inherited type I diabetes at an early age. ER-translocation-failed species of R6C insulin likely exhibit gain-of-function toxicity toward insulin-producing β cells (Guo et al., 2014), thereby causing a dominant effect to initiate type I diabetes. However, the mis-accumulation of unprocessed insulin in the cytoplasm is poorly characterized.

We confirmed that most newly translated insulin R6C mutants had impaired ER translocation, resulting in their cytoplasmic accumulation as non-processed prepro-type precursor forms in the presence of the protease inhibitor MG-132 (Fig. S2, E and F) (Guo et al., 2014; Braunstein et al., 2015). We found that Flag-tagged TanGIBLE co-precipitated more with prepro-insulin R6C than with BAG6 N200 (Fig. S2 G, compare lanes 15 and 16). R6C prepro-insulin co-precipitation with TanGIBLE was greatly enhanced in the presence of MG-132 (Fig. 3 A, compare lanes 12 and 16), suggesting that TanGIBLE recognizes a very unstable pool of defective secretory proteins. Quantification of the signal intensity of prepro-insulin suggested that TanGIBLE co-precipitated >9.6-fold more R6C mutant insulin compared with the BAG6 N200 fragment.

We further validated the specificity of TanGIBLE for capturing defective insulin species by developing a mutated version of the probe, designated 10S TanGIBLE, as a negative control. As shown in Fig. 3, B a, surface-exposed hydrophobic residues in the UBL domains (corresponding to Ile^{32}, Ile^{60}, Val^{65}, and Val^{81} of human BAG6, indicated in red characters in Fig. 3, B b) were simultaneously substituted with hydrophilic serine (indicated in blue in Fig. 3, B b) in 10S TanGIBLE. In addition to these mutations, 10S TanGIBLE also possesses 6S mutations (six critical hydrophobic residues in the BUILD domains were substituted with serine, Fig. 2 B and Fig. 3, B c) (Tanaka et al., 2016). The 10S TanGIBLE fragment lost its affinity for R6C prepro-insulin nearly completely, even in the presence of a protease inhibitor (Fig. 3 C, compare lanes 5 and 6).

Prolonged exposure of the blot revealed that TanGIBLE precipitates R6C insulin with multiple ladders visible via western blot at ∼8 kDa intervals (Fig. 3 D, blue arrowheads in lane 3), suggesting that TanGIBLE exhibits affinity for the covalently modified prepro-form. In contrast, 10S TanGIBLE did not co-precipitate ladder-like signals of defective insulin (Fig. 3 D, lane 2), suggesting that the hydrophobic residues in the UBL and BUILD domains are critical for target discrimination. Taken together, TanGIBLE is useful for evaluating the accumulation of mislocalized secretory proteins whose cytoplasmic accumulation causes neonatal onset of type I diabetes.

TanGIBLE captures neurodegeneration-causing defective prion protein (PrP)

PrP is a disease-associated glycosylphosphatidylinositol (GPI)-anchored glycoprotein whose misaccumulation in an aberrant structure may cause fatal neurodegenerative disorders in humans and mice (Chakrabarti et al., 2009, 2011). Hegde and colleagues reported that the ER-translocation efficiency of PrP SS is low in nature and that a non-negligible portion of PrP is produced as a mislocalized protein in the cytosol, especially under stress conditions (Rane et al., 2004; Levine et al., 2005; Kang et al., 2006; Hessa et al., 2011; Rodrigo-Brenni et al., 2014). To examine whether TanGIBLE can discriminate mislocalized species of human PrP, we compared two previously established mutants, N3a-PrP and Prl-PrP (Kim et al., 2002; Rane et al., 2004). N3a-PrP possesses point mutations within its SS (Fig. S2 H, indicated in red), and its efficiency for ER translocation is compromised compared with the WT protein. In contrast, Prl-PrP possesses a highly efficient SS derived from prolactin (Prl) in place of the native SS (Fig. S2 H) (Kim et al., 2002; Rane et al., 2004). Prl-PrP is produced as a glycosylated species (Fig. 3 E, blue line in input lane 3), suggesting that the most newly synthesized Prl-PrP is successfully translocated into the ER lumen. Importantly, TanGIBLE did not retrieve any of these glycosylated forms of Prl-PrP (Fig. 3 E, blue line in IP lane 6), but non-glycosylated species co-precipitated with TanGIBLE (Fig. 3 E, indicated by black arrowheads). Co-precipitation of N3a-PrP with TanGIBLE is dependent on the presence of MG-132 (Fig. 3 F, compare lanes 9 and 10), and a portion of the co-precipitated N3a-PrP was covalently modified (Fig. 3 E, red arrowheads in IP lane 5). These ladder-like signals were weakened by 4 h treatment with MLN7243 (TAK-243), an inhibitor of the ubiquitin-activating E1 enzyme (Fig. S2 I), suggesting that some of the TanGIBLE-associated N3a-PrP was ubiquitinated. In contrast, 10S TanGIBLE did not co-precipitate N3a-PrP, even in the presence of MG-132 (Fig. 3 F, compare lanes 10 and 11). These results indicate that TanGIBLE can discriminate neurodegeneration-causing cytotoxic species of PrP destined for proteasomal degradation.

TanGIBLE retrieves endogenous polyubiquitinated species induced by heat stress

Given that TanGIBLE was found to recognize a variety of model defective proteins (Figs. 2 and 3), and that co-precipitated defective translational products, such as R6C insulin and N3a-PrP, were covalently modified (Fig. 3, D and E, Hessa et al., 2011; Suzuki and Kawahara, 2016), we were interested in ascertaining whether TanGIBLE has an affinity for endogenous defective proteins with polyubiquitin modifications. Therefore, we investigated the possible interaction between TanGIBLE and defective species induced by heat stress, which is known to stimulate the accumulation of structurally defective polyubiquitinated polypeptides (Parag et al., 1987; Fujimuro et al., 1997).

Flag-tagged TanGIBLE, N200, and N200-6S mutant fragments were expressed with T7-tagged ubiquitin in HeLa cells, then the cells were cultured either at 44°C (heat stress) or 37°C (control) for 1 h without proteasome inhibitor treatment. Flag-tagged TanGIBLE co-immunoprecipitated T7-tagged proteins under heat stress (Fig. 4 A, lane 8) and retrieved more of these heat-shock-induced polyubiquitinated species than the N200 fragment (Fig. 4 A, compare lanes 6 and 8). The N200-6S mutant (Fig. 2 B) co-precipitated less of the polyubiquitinated client

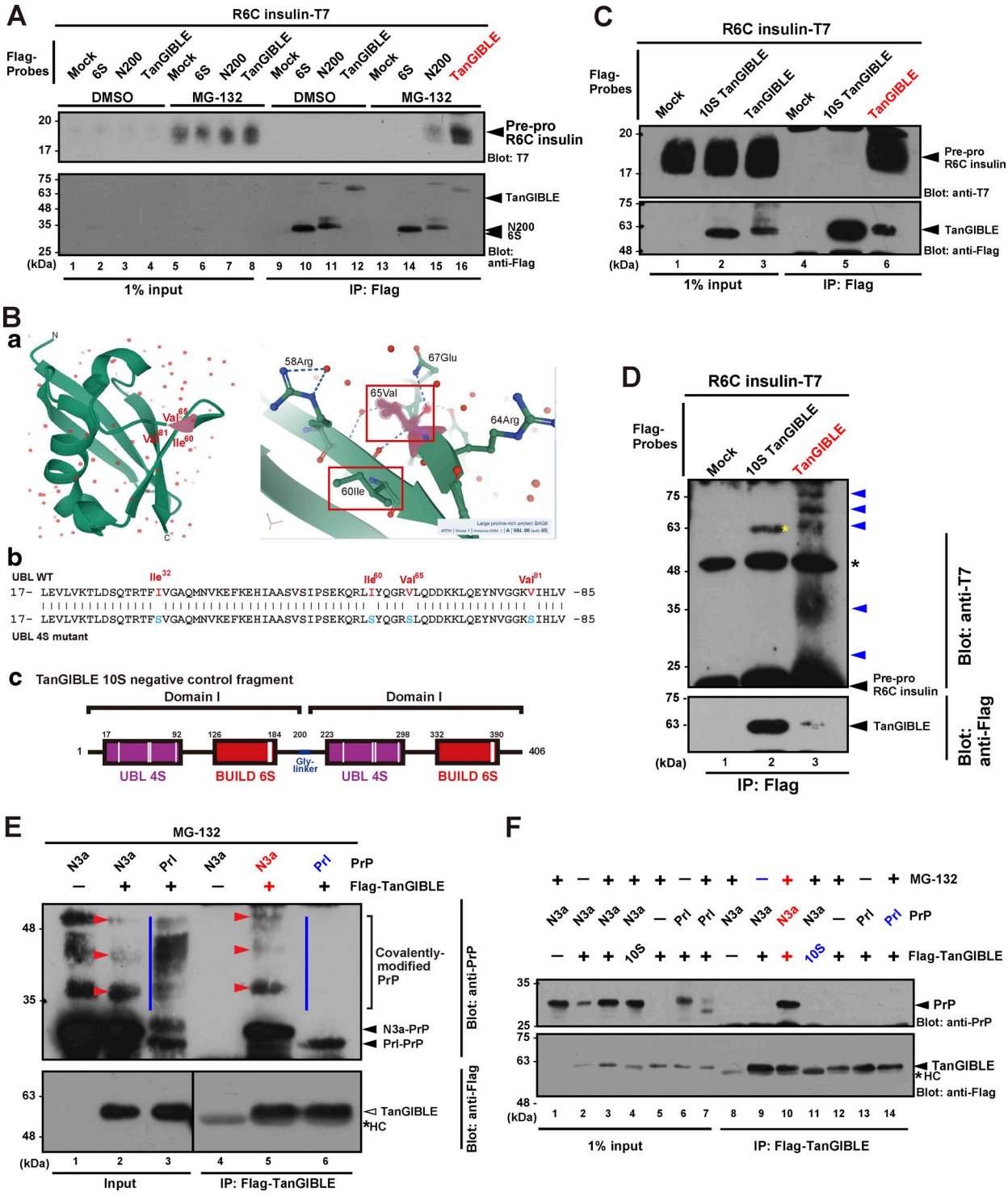

Figure 3. **Disease-associated defective proteins were captured by TanGIBLE. (A)** TanGIBLE interacts with the translocation-defective prepro-form of insulin mutants. HeLa cells expressing C-terminally T7-tagged insulin WT or R6C and Flag-tagged TanGIBLE were treated with 10 μM MG-132, as indicated. At 4 h after MG-132 treatment, the cells were lysed and immunoprecipitated (IP) with anti-Flag M2 agarose beads. Precipitates were blotted using the indicated antibodies. **(B)** Schematic of the 10S TanGIBLE developed as a negative control in this study. **(a)** Reported structure model of the UBL domain of BAG6 (PDB: 4EEW). The side chains of the Ile^{60}, Val^{65}, and Val^{81} residues in the BAG6 UBL domain are exposed on the surface of the domain and make a closely associated hydrophobic cluster. Note that Ile^{60} of BAG6 UBL corresponds to the ubiquitin Ile^{44} critical for ubiquitin-mediated protein–protein interactions. Except for Ile^{60}, the hydrophobicity of these residues (Ile^{32}, Val^{65}, and Val^{81}) is highly conserved in BAG6 orthologs from various vertebrates but is not conserved in ubiquitin and other UBL proteins, suggesting that the surface-exposed hydrophobicity is BAG6 UBL-specific. **(b and c)** Since the tandemly aligned N200-6S fragment was found to show non-negligible binding ability with model defective proteins, we further introduced mutations in the UBL domain. Four conserved hydrophobic residues in the UBL domain (correspond to Ile^{32}, Ile^{60}, Val^{65}, and Val^{81} of human BAG6, indicated in red characters), as well as six hydrophobic residues in the BUILD domain (identical to the N200-6S mutations, see Fig. 2 B), were substituted simultaneously with hydrophilic serine residues. The

tandemly aligned fragment with these mutated domains was designated 10S TanGIBLE and verified as a negative control. **(C and D)** HeLa cells expressing C-terminally T7-tagged R6C insulin, Flag-tagged TanGIBLE, and its 10S negative control fragment were treated with 10 µM MG-132, and Flag-precipitates were blotted using the indicated antibodies. TanGIBLE co-precipitated R6C insulin, while 10S mutated TanGIBLE did not. Prolonged exposure of the same blot showed ladder-like modifications of prepro-insulin exclusively in the TanGIBLE precipitates (D, lane 3). Yellow and black asterisks indicate non-specific and immunoglobulin signals, respectively. **(E)** HeLa cells expressing Flag-tagged TanGIBLE, T7-tagged N3a-PrP, and Prl-PrP were treated with 10 µM MG-132, and Flag-precipitates were blotted using anti-PrP antibody. Note that N3a-PrP was co-precipitated with TanGIBLE with multiple ladder-like signals (indicated with red arrowheads), whereas very little glycosyl-modified Prl-PrP co-precipitated with TanGIBLE (indicated by blue lines). Unmodified PrP species are indicated with black arrowheads. **(F)** TanGIBLE co-precipitated N3a-PrP in the presence of MG-132, while 10S mutated TanGIBLE did not precipitate N3a-PrP, even with MG-132. Asterisk indicates signal of immunoglobulin. Source data are available for this figure: SourceData F3.

proteins from cell extracts under identical conditions (Fig. 4 A, compare lanes 4 and 8). To verify whether TanGIBLE can retrieve endogenous defective proteins, we probed TanGIBLE precipitates with an anti-polyubiquitin FK2 antibody (Fujimuro et al., 1997). The results clearly showed that TanGIBLE detects FK2 antigens induced by heat stress (Fig. 4 B), suggesting that this new probe can retrieve endogenous polyubiquitinated defective proteins.

TanGIBLE retrieves newly synthesized polypeptides destined for ubiquitin-dependent degradation

Similar to the case with heat stress, proteasome inhibition stimulated the accumulation of endogenous polyubiquitinated proteins. We found that TanGIBLE retrieved a part of endogenous polyubiquitinated proteins from MG-132–treated HeLa cells (Fig. 4 C, lane 6). As a negative control for polyubiquitin co-precipitation, 10S TanGIBLE lost its affinity with polyubiquitinated species even in the presence of MG-132, in contrast with the results obtained using authentic TanGIBLE (Fig. 4 C, compare lanes 5 and 6).

We next asked if TanGIBLE is itself polyubiquitylated. As a positive control, we confirmed that the proteasome substrate Rab8a T22N is covalently modified with polyubiquitin since denaturation with 1% SDS at 90°C did not abolish polyubiquitin co-precipitation with Rab8a T22N (Fig. S3 A, lane 8, Takahashi et al., 2019, 2023). In contrast, polyubiquitin chains associated with TanGIBLE completely disappeared from immunoprecipitates following their denaturation to abolish noncovalent protein–protein interactions (Fig. S3 A, lane 6). The UBA-domain protein UBQLN4 was used as a negative control for covalent polyubiquitination. These observations suggest that TanGIBLE itself does not undergo covalent polyubiquitin modification. In accordance with this notion, cycloheximide (CHX, a protein synthesis inhibitor) chase experiment provided support that TanGIBLE is a long-lived protein in cells (Fig. S3 B). We concluded that hydrophobicity-mediated noncovalent interactions are essential for the association between TanGIBLE and its endogenous polyubiquitinated clients destined for degradation.

Polyubiquitinated proteins in proteasome-suppressed cells include not only newly synthesized proteins but also structurally normal proteins. MHC class I–restricted antigenic peptides are reportedly derived from the degradation products of newly synthesized defective polypeptides, which are sensitive to protein synthesis inhibitors (Yewdell, 2011). To elucidate whether co-precipitates of TanGIBLE contain newly synthesized short-lived polypeptides as clients, we examined the effects of a protein synthesis inhibitor. We found that treatment with CHX largely abolished polyubiquitin co-precipitation with TanGIBLE (Fig. 4 D, compare lanes 3 and 4 in the upper IP panel, see also Fig. S3 C, compare lanes 3 and 7), even though the total amount of ubiquitinated protein in the whole-cell lysate was essentially unaffected by CHX (Fig. 4 D, middle input samples, compare lanes 3 and 4). These observations suggest that CHX-sensitive newly synthesized defective ribosomal products are the major targets of TanGIBLE.

Liquid chromatography-tandem MS (LC-MS/MS)–based identification of endogenous defective proteins trapped by TanGIBLE

We next examined whether TanGIBLE can be used to identify an uncharacterized endogenous defective protein pool. For this purpose, we used Flag-tagged TanGIBLE for the in-cell capture of polyubiquitinated polypeptides from HeLa cell extracts (Fig. 5 A for FK2 western blot, Fig. S4 A for silver stain). The Flag-immunoprecipitates were subjected to LC-MS/MS (Fig. 5, B and C, see also Fig. S4 B). Three biologically independent analyses resulted in the identification of more than 1,000 candidate proteins as endogenous targets of TanGIBLE (Table S1). We selected candidate defective proteins whose MS scores increased in MG-132–treated cells (Fig. 5 B, 143 candidates with a P value <0.05) but decreased in 10S TanGIBLE precipitation (Fig. 5 C, 142 candidates with a P value <0.05). Of these, 101 candidates were sensitive to both MG-132 treatment and 10S mutation at significant levels. It is noteworthy that most of these candidate proteins were either membrane proteins (colored light blue, Fig. 5 D) or subunits derived from multiprotein complexes (colored light pink, Fig. 5 D).

Of these candidate membrane proteins, we chose basigin, an immunoglobulin superfamily transmembrane protein, as the first example of an endogenous defective protein because of its high reproducibility in MS analyses (a P value of $<10^{-4}$), and because defective species and successfully synthesized counterparts can be readily distinguished. Basigin belongs to the ER-resident membrane protein family, and its successful biosynthesis can be monitored by its characteristic smear signals through anti-basigin western blot analysis (corresponding to the degree of glycosylation, Fig. 5 E, indicated by a yellow line on lane 3) (Muramatsu, 2016). TanGIBLE selectively retrieved the non-glycosylated species of endogenous basigin (Fig. 5 E, indicated by a red arrowhead in the IP lane). In contrast, the major glycosylated (successfully synthesized) species of basigin was essentially not recognized by TanGIBLE (Fig. 5 E, indicated by a yellow line in the IP lane), suggesting that TanGIBLE showed a strong preference for defective species of endogenous basigin. In

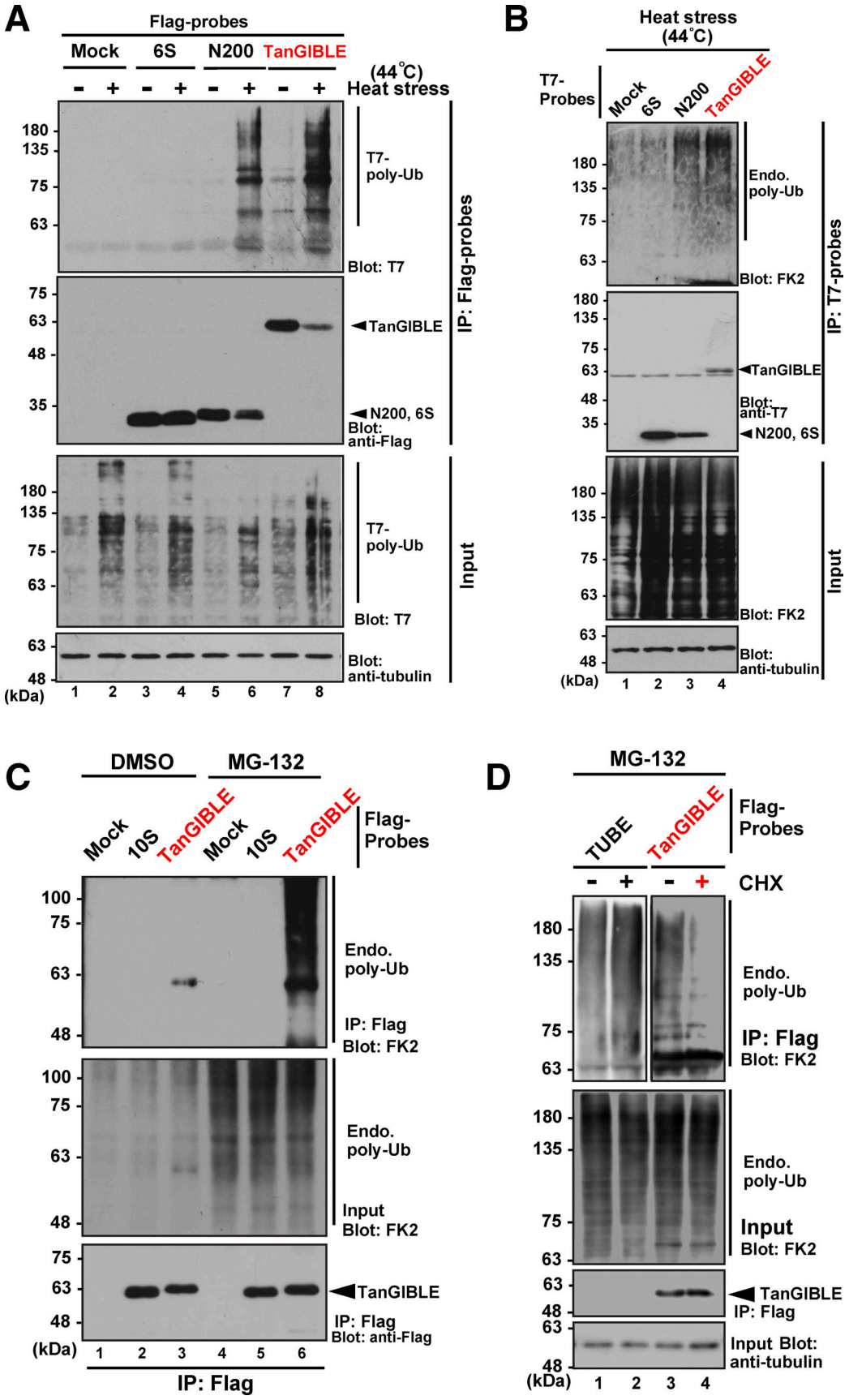

Figure 4. **Newly synthesized defective polypeptides are endogenous clients of TanGIBLE. (A)** TanGIBLE retrieves heat shock–induced polyubiquitinated proteins. HeLa cells were co-transfected with Flag-tagged TanGIBLE and T7-tagged ubiquitin, and these cells were cultured at 44°C (heat stress, +) or 37°C

(without heat stress, –) for 1 h without the proteasome inhibitor. After heat shock treatment, Flag-tagged probes were immunoprecipitated (IP) and blotted with anti-T7 antibody. Mock indicates empty vector transfection. **(B)** T7-tagged TanGIBLE can co-precipitate endogenous polyubiquitinated proteins after heat stress. TanGIBLE and its control probes were immunoprecipitated from heat-stressed cells using anti-T7 agarose beads, and co-precipitates of endogenous polyubiquitinated proteins were detected using anti-polyubiquitin FK2 antibody. α-Tubulin was used as the loading control. **(C)** HeLa cells expressing Flag-tagged TanGIBLE and its 10S negative control fragment were treated with 10 μM MG-132. Flag-precipitates were blotted using anti-polyubiquitin FK2 antibody (upper panel). **(D)** Polyubiquitinated proteins associated with TanGIBLE are sensitive to CHX. HeLa cells expressing Flag-tagged TanGIBLE or TR-TUBE were treated with 25 μg/ml CHX (or its solvent, EtOH) and then 10 μM MG-132 as indicated for 4 h, then were affinity-purified from the cell extracts using an anti-Flag antibody. Flag-precipitates (IP: Flag) were blotted with anti-polyubiquitin FK2 antibody to detect co-precipitated endogenous polyubiquitinated proteins. Source data are available for this figure: SourceData F4.

agreement with this idea, TanGIBLE-associated basigin did not respond to deglycosylation reaction (Fig. S4 C, compare lanes 5 and 6). Importantly, TanGIBLE-associated basigin can be largely upregulated by MG-132 (Fig. 5 E, compare lanes 7 and 8) and is sensitive to CHX treatment (Fig. S4 D, compare lanes 8 and 9), suggesting that this is an unstable newly synthesized species. In contrast, glycosylated (successfully synthesized) basigin in whole-cell lysates was insensitive to MG-132 (Fig. 5 E, compare lanes 2 and 3). We confirmed that 10S TanGIBLE recognized much smaller amounts of endogenous basigin than did authentic TanGIBLE (Fig. 5 E, compare lanes 8 and 9). Another transmembrane protein BST2, in its non-glycosylated form, was also co-immunoprecipitated specifically with TanGIBLE (Fig. S4 E). These observations support the view that the TanGIBLE probe coupled with LC-MS/MS–based analysis provided a new and effective way to identify uncharacterized defective species of endogenous proteins from small amounts of cell lysate. We also confirmed that the forced expression of TanGIBLE in HeLa cells did not affect the expression level of endogenous tail-anchored protein SEC61β, a critical translocon subunit (Fig. S3 D), and did not affect glycosyl modifications of opsin-tagged SEC61β (Fig. S3 E), suggesting that the translocon machinery is intact in TanGIBLE expressing cells.

Tandem ubiquitin-binding entities (TUBE) have been developed for the MS-based analysis of ubiquitinated proteins (Hjerpe et al., 2009; Yoshida et al., 2015) and should be an important comparison to the TanGIBLE probe. Flag-tagged TR-TUBE (trypsin-resistant TUBE, Yoshida et al., 2015) was found to co-precipitate a much larger amount of target protein (compare estimated protein concentrations in TanGIBLE WT and TR-TUBE in Fig. S4 A) and reacts far more strongly with FK2 anti-polyubiquitin antibody than does TanGIBLE (Fig. 5 A, compare lanes 3 and 5). However, the polyubiquitin signals that co-precipitated with TR-TUBE were unaffected by CHX treatment (Fig. 4 D, compare lanes 1 and 2), whereas the signals with TanGIBLE were highly sensitive to CHX (Fig. 4 D, compare lanes 3 and 4 in upper panel). These observations suggest that a major portion of the TR-TUBE clients was derived from CHX-insensitive polypeptides, in contrast to the TanGIBLE clients. The ratios of TanGIBLE-preferred clients to TR-TUBE–preferred clients were different, and many of the TanGIBLE-preferred proteins could be identified by MS analysis (Fig. 5 F). For example, basigin was identified as a TanGIBLE-preferred endogenous client (Fig. 5, E and F), while TR-TUBE recognized less non-glycosylated basigin (Fig. 5 E, compare lanes 8 and 10). Thus, although TUBE is an efficient probe for recovering ubiquitinated proteins in general, TanGIBLE more preferentially retrieves newly synthesized defective species such as non-glycosylated endogenous basigin (Fig. 5 G).

Orphaned minichromosome maintenance (MCM) subunits are endogenous defective proteins identified by TanGIBLE

The candidate defective proteins retrieved by TanGIBLE included many endogenous subunits of multiprotein complexes (Fig. 5 D), such as molecular chaperone CCT/TRiC complex (all eight subunits were identified in TanGIBLE precipitates, Fig. 6, A a), RNA polymerase II complex (8 of 12 subunits were identified, Fig. 6, A b), and MCM complex (all six subunits were identified, Fig. 6, A c and d). All these co-precipitations with TanGIBLE were strengthened by proteasome inhibition and weakened when 10S mutated TanGIBLE was used (Fig. 6 A). CCT/TRiC complex was recently reported as a source of orphaned defective proteins if the expression of these proteins is perturbed (Yagita et al., 2023). In this study, we focused on the MCM protein complex because all six endogenous MCM subunits were identified by MS analyses of TanGIBLE precipitates in an MG-132–dependent manner (Fig. 6, A c). Western blot analysis with anti-MCM6 antibody showed that endogenous MCM6 co-immunoprecipitated with TanGIBLE from HeLa cell extracts, similar to the case for defective basigin detected on the same blot (Fig. 6 B). 10S mutation in TanGIBLE abolished its affinity for endogenous MCM6 (Fig. 6 B, compare lanes 8 and 9). MCM6 immunosignals co-precipitated with TanGIBLE were weakened by MCM6 siRNA (Fig. S4 F), confirming that these signals were specific.

MCM is a six-membered ring protein complex (Fig. 6, A d) (Deegan and Diffley, 2016; Akopian and Rape, 2017), and the forced depletion of any single subunit were reported to cause the pan-destabilization of the other MCM subunits (Ibarra et al., 2008; Ge et al., 2007). Thus, the hexameric stoichiometry of the MCM subunit complex should be strictly adjusted. We thus chose this complex as a model for studying the production of unstable orphans derived from the unbalanced synthesis of subunits. We examined whether TanGIBLE recognizes the orphaned MCM6 subunit by depleting the MCM2 subunit in HeLa cells and the TanGIBLE immunoprecipitates were blotted with anti-MCM6 antibody. The amount of endogenous MCM6 co-precipitated with TanGIBLE was increased by MCM2 depletion (Fig. 6 C, compare lanes 2 and 3 in the upper IP panel), despite a marked reduction in the total endogenous MCM6 subunit following disruption of the complex by MCM2 siRNA (Fig. 6 C, input panel) (Ge et al., 2007; Ibarra et al., 2008). Furthermore, endogenous MCM6 subunits associated with TanGIBLE were sensitive to MG-132 or CHX treatment in the presence of MCM2

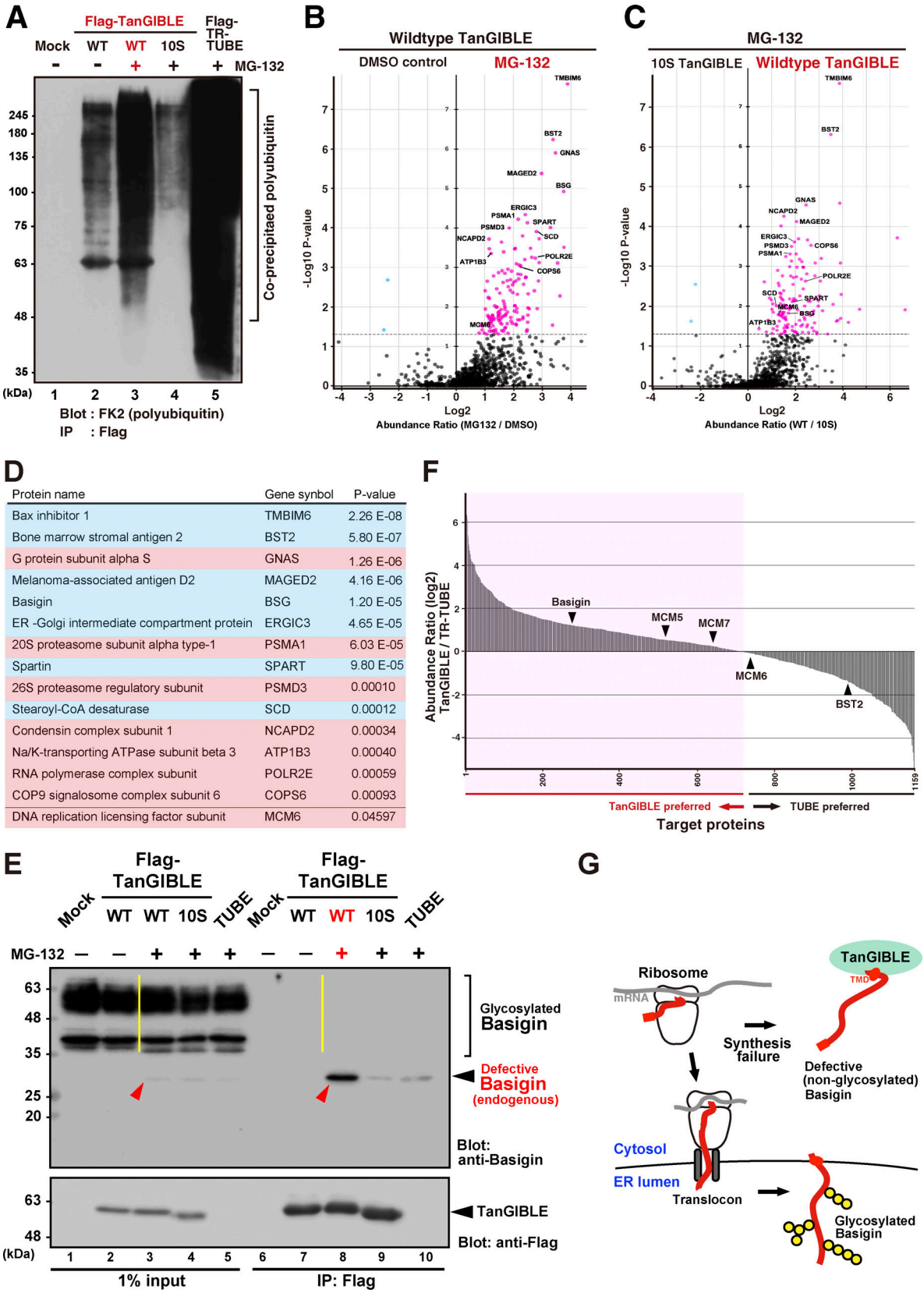

Figure 5. **LC-MS/MS–based identification of defective proteins trapped by TanGIBLE. (A)** Flag-immunoprecipitates from MG-132–treated HeLa cell lysates were blotted with anti-polyubiquitin FK2 antibody. Identical precipitates were silver-stained in Fig. S4 A. **(B and C)** TanGIBLE-immunoprecipitates shown in A were directly subjected to LC-MS/MS analysis. Volcano plots of TanGIBLE-immunoprecipitates identified by deep MS analysis, highlighting enriched or lost proteins with or without MG-132 protease inhibitor treatment (B). Lanes 2 and 3 shown in A correspond to "DMSO control" and "MG-132," respectively.

Volcano plots highlighting enriched or lost proteins in the 10S TanGIBLE interactome compared with authentic TanGIBLE (C). Lanes 3 and 4 shown in A correspond to "Wildtype TanGIBLE" and "10S TanGIBLE," respectively. **(D)** Representative list of TanGIBLE target proteins identified by triplicate MS analyses. P values of abundance ratio (MG-132 versus DMSO treatments) were indicated. Transmembrane proteins are colored light blue and the subunits of multi-protein complexes are colored light pink. **(E)** Endogenous basigin with no glycosyl modifications (indicated by red arrowheads) was predominantly co-immunoprecipitated (IP) with Flag-TanGIBLE in an MG-132–dependent manner (lane 8). Note that successfully synthesized basigin (indicated by a yellow line in the input lane 3) was not detected in identical precipitates (yellow line in the IP lane 8). Basigin co-precipitations were largely compromised in the 10S TanGIBLE and TR-TUBE precipitations (lanes 9 and 10). **(F)** Abundance ratio (log_2) histogram of TanGIBLE/TR-TUBE immunoprecipitates. TR-TUBE–preferred targets are shown on the right and TanGIBLE-preferred proteins are shown on the left. Note that ∼2.5-fold more TUBE-associated polyubiquitinated proteins were subjected to MS analyses compared to the amount of protein co-precipitated with TanGIBLE (Fig. S4 A). We therefore adjusted the threshold (cutoff) for TanGIBLE-preferred proteins accordingly. **(G)** Schematic of the successful assembly of glycosylated basigin into the ER. Note that failure of ER assembly resulted in glycosylation defects, and non-glycosylated defective basigins were trapped by the TanGIBLE. Source data are available for this figure: SourceData F5.

siRNAs (Fig. 6 C, compare lanes 1 and 3, Fig. S4 G, compare lanes 2 and 5). Similar results were obtained with other MCM subunits; TanGIBLE-associated MCM7 and MCM5 were augmented upon MCM2 depletion (Fig. 6 D and Fig. S4 H, top IP panels) despite large reductions in total endogenous MCM7/5 subunits in cells using MCM2 siRNA (Fig. 6 D and Fig. S4 H, input panel). TanGIBLE-associated species of MCM7/5 proteins were also highly sensitive to MG-132 (Fig. 6 D and Fig. S4 H). These results collectively suggest that TanGIBLE retrieved unstable (i.e., MG-132 sensitive) and newly synthesized (i.e., CHX sensitive) endogenous pools of orphaned MCM subunits.

It should be noted that intersubunit associations between neighboring MCM subunits are mediated through hydrophobic interactions (Li et al., 2015). For example, Met^{342} and Phe^{391} of yeast MCM4 and Ile^{284} of yeast MCM6 (these are conserved as Met^{299} and Phe^{346} in human MCM4 and Ile^{131} in human MCM6, respectively) are critical for direct interaction between the subunits (Li et al., 2015). These results suggest that orphaned subunits lacking their binding partner tend to surface-expose these hydrophobic residues to the aqueous cytosol. Similarly, hydrophobic patches at the corresponding surfaces in human MCM subunits also tend to be exposed in the absence of their binding partner (Fig. S5). These exposed hydrophobic sites of orphaned MCM subunits might help drive TanGIBLE recognition. In agreement with this view, 10S mutated TanGIBLE did not co-precipitate with any MCM subunit tested (Fig. 6, C and D; and Fig. S4 F), suggesting that TanGIBLE indeed recognizes MCM subunits via their exposed hydrophobic residues.

TanGIBLE as a new probe for cytoplasmic foci composed of defective polypeptides

As one of the applications for this newly developed device, we investigated whether TanGIBLE can be utilized as a probe for defective nascent polypeptides in situ. Puromycin is an analog of aminoacyl tRNA and can be incorporated into newly synthesized polypeptides to terminate translation prematurely, thus leading to the mass production of truncated polypeptides in the cytosol. Such abnormal polypeptides tend to form a type of SGs, which are motile cytoplasmic foci for the transient storage of polyubiquitinated defective ribosomal products (Lelouard et al., 2002, 2004; Anderson and Kedersha, 2002; Szeto et al., 2006). We examined whether Flag-tagged TanGIBLE enables the visualization of accumulated puromycin-induced defective proteins by co-immunostaining with anti-Flag, anti-puromycin, and anti-polyubiquitin antibodies. To exclude the possibility that TanGIBLE is incorporated into the SGs as a C-terminally truncated non-functional species, we prepared a C-terminally tagged probe (designated as TanGIBLE-Flag). This ensured the FL translation of this probe, even with puromycin treatment. TanGIBLE-Flag successfully detected puromycin-labeled SGs that stained positive with anti-puromycin (Fig. 7 A, red for TanGIBLE-Flag and green for puromycin signals). The case was similar in the immunostaining of polyubiquitin, a conventional marker for puromycin-induced SGs (Fig. S6, A and B, green for TanGIBLE-Flag and red for anti-polyubiquitin signals). Although most of the foci are double-positive for FK2 and TanGIBLE stains, their green/red signal intensity ratios varied on respective foci. Note that the exposure times for the TanGIBLE stain photographs were almost one-tenth that for the FK2 polyubiquitin stain, suggesting that TanGIBLE-Flag has higher detection sensitivity for foci compared with conventional ubiquitin immunostain. We also showed that N-terminally Flag-tagged TanGIBLE identified SGs as efficiently as its C-terminally tagged counterpart (Fig. S6 B). These observations suggest that TanGIBLE is advantageous for visualizing endogenous cytoplasmic foci that contain newly synthesized and prematurely truncated defective polypeptides compared with non-selective polyubiquitin antibodies.

TanGIBLE enables the visualization of real-time processes in cytoplasmic foci formations in living cells

Since TanGIBLE is a protein probe, it can be fused with any functional amino acid sequence to target specific potential applications. To explore this possibility, we fused TanGIBLE with fluorescent tags (such as EGFP or mCherry) for in situ imaging of endogenous defective proteins in living cells. As a first trial with fluorescent tag-fused TanGIBLE, we examined the behavior of TanGIBLE-EGFP to investigate whether TanGIBLE can detect the dynamic behavior of motile cytoplasmic foci that serve as transient storage for defective proteins. After allowing time for TanGIBLE-EGFP translation, we pulsed the cells with puromycin. Within 30 min of puromycin addition, cytoplasmic foci can be detected by TanGIBLE-EGFP, with the number and size increasing rapidly (Fig. 7 B, upper panel; see also Video 1). This observation suggests that TanGIBLE can detect very early stages of defective protein accumulation. These signals are specific, given that EGFP-tagged 10S TanGIBLE did not show cytoplasmic foci under identical conditions (Fig. 7 B, middle panels; see also

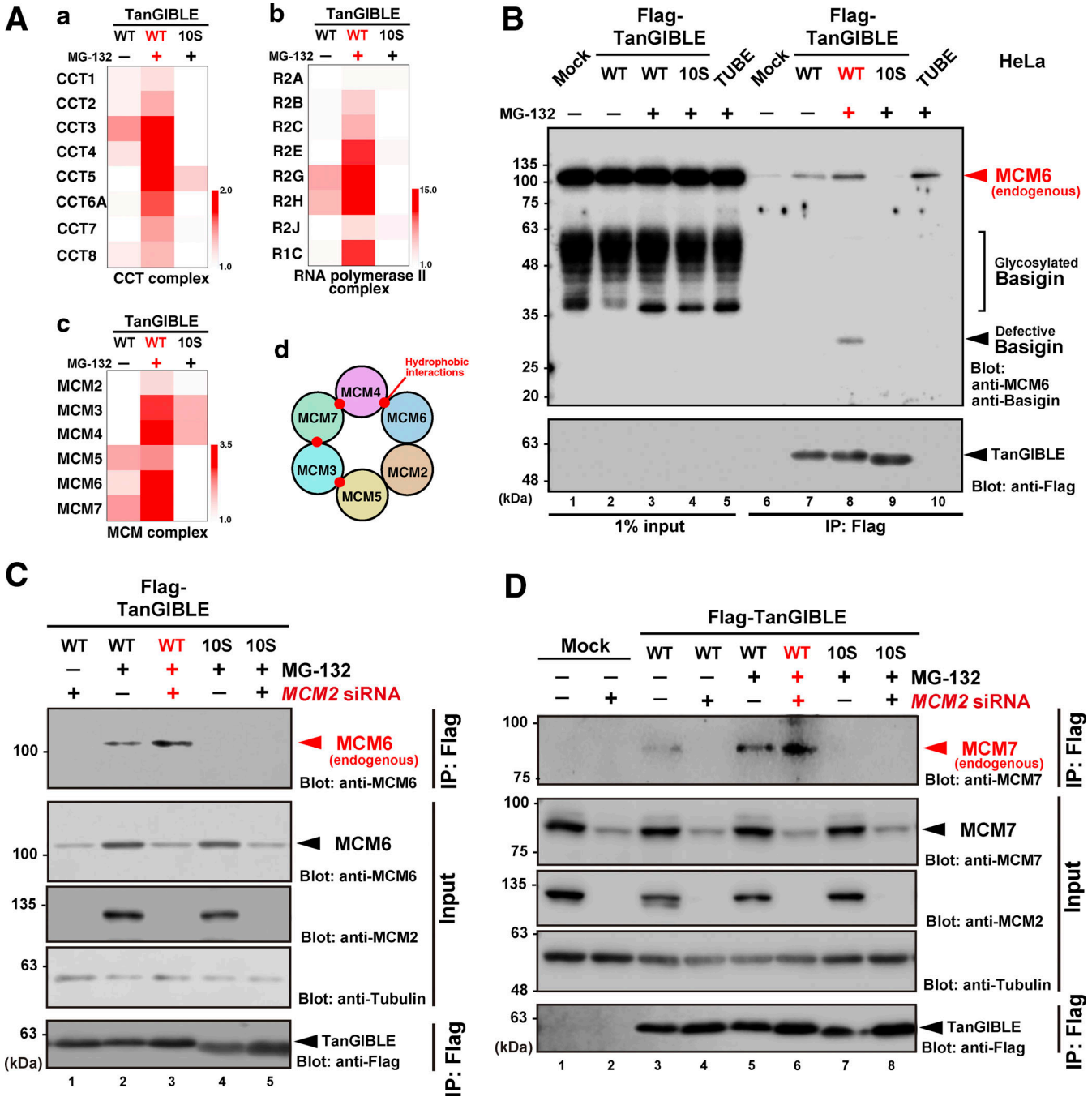

Figure 6. **Endogenous orphaned subunits derived from MCM complex are targets of TanGIBLE. (A, a–c)** Heat maps of the subunits of CCT/TRiC complex (a), RNA polymerase II complex (b), and MCM complex (c), which were identified by MS analysis of TanGIBLE immunoprecipitates (IP). All subunits in the precipitates were augmented in the presence of MG-132 but were decreased with 10S mutations of the TanGIBLE probe. Panel colors show the relative fold increase compared with the base line (defined as 1.0). Schematic of MCM hexamer complex model (d). Reported hydrophobic interactions are indicated as red dots. **(B)** HeLa cells expressing 3xFlag-tagged TanGIBLE were lysed and immunoprecipitated with anti-Flag M2 antibody and the eluted endogenous proteins were simultaneously immunoblotted with anti-basigin and anti-MCM6 antibodies. Defective basigin (indicated by a black arrowhead) and MCM6 (indicated by a red arrowhead) were detected in WT TanGIBLE with MG-132 treatment. Note that 10S TanGIBLE did not co-precipitate defective basigin and endogenous MCM6. **(C)** Orphaned MCM6 subunit derived from disrupted complexes is a target of TanGIBLE. The total amount of MCM6 protein was greatly reduced by *MCM2* siRNA (compare lanes 2 and 3 in input panel), whereas endogenous MCM6 co-precipitated with TanGIBLE is augmented by MCM2 depletion (compare lanes 2 and 3 in Flag IP panel). Note that MG-132 treatment did not restore the total amount of MCM6 protein significantly because MG-132–treated time (4 h) was too short to restore the total amount of MCM6 compared with the long period of MCM2 knockdown (72 h). Tubulin is shown as a loading control for input samples. **(D)** Augmentation of the endogenous MCM7 subunit level in a TanGIBLE immunoprecipitate after *MCM2* siRNA treatment (compare lanes 5 and 6 in Flag IP panel), even though the total amount of MCM7 protein is greatly reduced by *MCM2* siRNA (compare lanes 5 and 6 in input panel). Note that TanGIBLE-associated MCM7 is MG-132 sensitive (compare lanes 4 and 6 in Flag IP panel), while total MCM7 (shown in input panel) did not respond to short-term MG-132 treatment (4 h). Source data are available for this figure: SourceData F6.

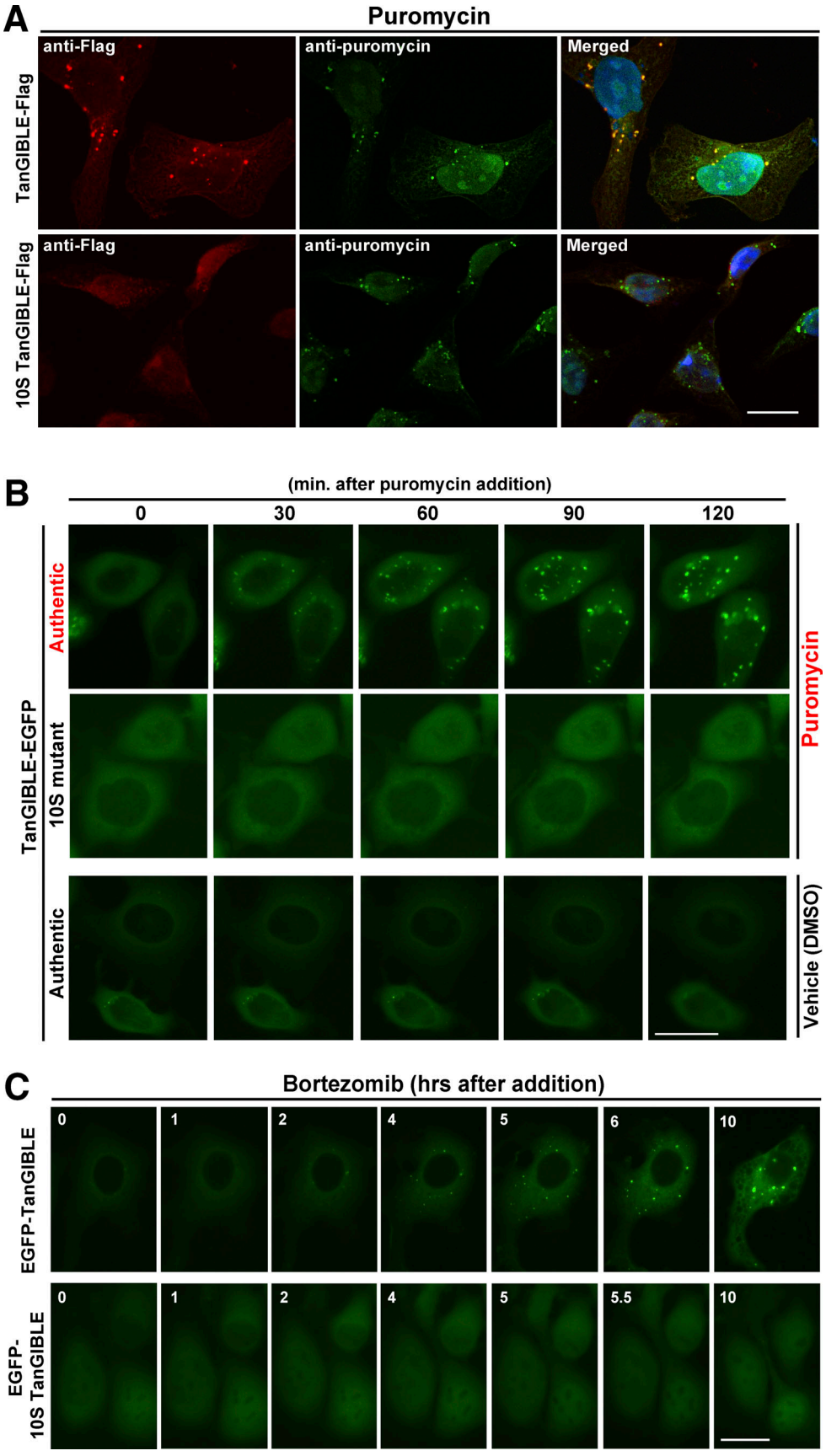

Figure 7. **Real-time detection of cytoplasmic foci induced by proteotoxic stresses. (A)** TanGIBLE can detect cytoplasmic foci composed of defective proteins. HeLa cells expressing C-terminally Flag-tagged TanGIBLE were treated with 10 µg/ml puromycin for 2 h, followed by 1% Triton X-100 extraction and

4% paraformaldehyde fixation. Fixed cells were stained with anti-Flag polyclonal (shown in red to detect TanGIBLE) and anti-puromycin (shown in green to detect puromycin-labeled defective proteins) antibodies. 10S TanGIBLE was used as a negative control. Scale bar: 20 µm. **(B)** Live cell detection of endogenous defective proteins induced by puromycin using EGFP-fused TanGIBLE. HeLa cells expressing EGFP-fused authentic TanGIBLE showed diffuse fluorescent signals throughout the cytoplasm. However, small cytoplasmic foci appeared within 30 min of puromycin treatment (5 µg/ml) and increased in size and number thereafter (upper panels). EGFP-fused 10S TanGIBLE was used as a negative control (middle panels). Authentic TanGIBLE did not cause cytoplasmic foci formation in the absence of puromycin (lower panels). Video images were available in Video 1 (EGFP-TanGIBLE) and Video 2 (EGFP-10S TanGIBLE). Scale bar: 20 µm. **(C)** Live cell detection of endogenous defective proteins induced by bortezomib treatment using EGFP-fused TanGIBLE. In HeLa cells expressing EGFP-TanGIBLE, small cytoplasmic foci appeared after 4 h of bortezomib treatment (10 µM) and increased in size thereafter. EGFP-fused 10S TanGIBLE was used as the negative control. Scale bar: 20 µm.

Video 2). In addition, we also confirmed that only a small number of TanGIBLE-derived foci were observed following solvent vehicle treatment (e.g., 1% DMSO), even with prolonged observation times (Fig. 7 B, lower panel), excluding the possibility that TanGIBLE itself was aggregated. These results suggest that fluorescent protein-fused TanGIBLEs enabled us to visualize the formations of cytoplasmic foci of hydrophobicity-exposed defective proteins in a real-time manner, presenting the opportunity to investigate the early stage of endogenous defective protein accumulation at a single living cell level under stress conditions.

Finally, we examined the behavior of EGFP-TanGIBLE in bortezomib-treated HeLa cells. Inhibition of the proteasome is known to promote the accumulation of aggregation-prone defective proteins (Johnston et al., 1998). Although TanGIBLE itself is a highly stable protein (Fig. S3 B), we found that EGFP-TanGIBLE can detect aggresome-like structures induced by bortezomib treatment at the periphery of the nucleus (Fig. 7 C), suggesting that this probe can visualize the process of defective protein aggregation in real-time.

Discussion

We provided evidence that TanGIBLE can recognize a variety of model defective proteins, such as polypeptides derived from frame-shifted translation (Fig. S2, A and B), translocon-rejected TMD proteins (Fig. 2 and Fig. S1, B–D), human disease-associated secretory proteins (Fig. 3, A, C, and D), and GPI-anchored proteins (Fig. 3, E and F). TanGIBLE captured not only these model aberrant proteins but also endogenous polyubiquitinated defective proteins, including species induced by heat stress (Fig. 4, A and B), proteasome inhibition (Fig. 4, C and D), and translational attenuation (Fig. 7, A and B). This versatility therefore enabled us to isolate (and visualize) as-yet-"hypothetical" existence of endogenous defective polypeptides as tangible entities. TanGIBLE allowed the retrieval of these defective species in the liquid phase and provided a novel method to profile elusive aberrant proteins using proteomics and imaging under various physiological and pathological conditions. These properties provide crucial insights into many areas of cell biology. We also developed an important negative control probe (10S TanGIBLE) to test the specificity of TanGIBLE.

An attractive hypothesis was proposed, suggesting that degradation products derived from newly synthesized defective polypeptides are the major source of antigenic peptides for MHC class I pathways (Yewdell et al., 2003; Yewdell, 2011). In accordance with this idea, proteasome or ribosome inhibition should efficiently block MHC class I–mediated antigen presentation. Pulse-labeling experiments showed that more than 5% (and up to 40%) of polypeptides are degraded immediately after ribosomal translation in mammalian cells (Schubert et al., 2000; Yewdell et al., 2003; Yewdell, 2011; Levine et al., 2005). In addition, a non-negligible portion of newly synthesized polypeptides is co-translationally ubiquitinated (Duttler et al., 2013; Wang et al., 2013). These findings are particularly important for viral immunity, given that some viral gene translation products are degradation-resistant if folded correctly, making it difficult to produce antigenic peptides from natively assembled viral proteins (Khan et al., 2001). Degradation products of defective ribosomal products are therefore suitable as major sources of antigenic peptides.

The exact identity of such rapidly degraded nascent polypeptides, however, remains largely obscure. This is partly because there has been no direct method for retrieving extremely divergent populations of labile defective species. To resolve this critical issue, we focused on the idea that misassembled polypeptides with aberrant structures tend to expose hydrophobic residues to the aqueous cytosol, and thus an affinity probe specific for hydrophobicity exposed to the cytosol would enable retrieval of these defective species. Related to this idea, recent unbiased genome-wide screening identified BAG6 as a top hit for the hydrophobicity surveillance of diverse noncoding genome translation (Kesner et al., 2023; Mohsen and Slavoff, 2023). It has also been reported that significant amounts of readthrough proteins arise when translational termination fails at stop codons (varying from <1% to over 10%), producing hydrophobic polypeptides encoded by the 3′-untranslated region (3′-UTRs) of mRNAs (Arribere et al., 2016; Müller et al., 2023). Such C-terminal extensions of model readthrough products are captured by BAG6, especially when their 3′-UTR products are enriched in hydrophobic amino acids (Müller et al., 2023). Similarly, Elledge and colleagues recently reported that CRISPR-mediated genome-wide screening identified BAG6 as a primary factor for the degradation of a variety of hydrophobic degron-containing model proteins recently identified by proteome-wide peptidome mapping (Zhang et al., 2023). They also noted that the degron motif recognized by BAG6 can be as short as three to four hydrophobic residues, in good accordance with our previous report (Kikukawa et al., 2005; Tanaka et al., 2016). Although all these studies utilized artificial polypeptides as model defective substrates, the substrate recognition motif of BAG6 could be an ideal tool for probing a wide variety of endogenous polypeptides with exposed hydrophobicity.

The problem was that BAG6 itself is a large, multidomain, and multifunctional protein that interacts with many accessory proteins, and their clients are not restricted to defective proteins (Kawahara et al., 2013). Fortunately, previous studies identified the minimum substrate-discriminating domain of BAG6, Domain I, which is dedicated to defective protein recognition (Kikukawa et al., 2005; Minami et al., 2010; Tanaka et al., 2016). This allowed us to develop a novel protein architecture, designated TanGIBLE, that can retrieve a variety of hydrophobicity-exposed defective polypeptides effectively.

Several lines of evidence suggest that the accumulation of defective proteins in cells may cause various human diseases, including prion disease (Rane et al., 2004, 2008, 2010; Chakrabarti et al., 2009), autosomal dominant late-onset diabetes (Skowera et al., 2008; Liu et al., 2012; Guo et al., 2014; Braunstein et al., 2015), altered presentation of T cell epitopes from viral proteins (Khan et al., 2001; Yewdell, 2011), and cancer etiology (Oromendia and Amon, 2014). Aneuploidy, an imbalance in the number of specific chromosomes, is a common feature observed in various diseases, such as cancer (Rajagopalan and Lengauer, 2004; Chunduri and Storchová, 2019). Aneuploidy disrupts protein homeostasis, and the resulting deleterious effects are believed to be linked to the accumulation of defective polypeptides (Stingele et al., 2012; Santaguida et al., 2015; Oromendia and Amon, 2014). Since aneuploidy causes the unbalanced expression of genes of multisubunit protein complexes, such as ribosome and MCM complexes, in which different subunits are encoded by genes on different chromosomes, this karyotype may stimulate the production of orphan subunits that lack their binding partners. Such orphaned subunits are supposed to be degraded immediately after synthesis or aggregated in the cytosol when they are not bound to their partners (McShane et al., 2016; Brennan et al., 2019; Zavodszky et al., 2021). Although the accumulation of such orphaned proteins may induce severe proteotoxic stress (Oromendia et al., 2012; Dephoure et al., 2014; Ben-David et al., 2014; Juszkiewicz and Hegde, 2018; Samant et al., 2019; Brennan et al., 2019), the exact identity of endogenous defective species in aneuploid cells is not adequately understood. These inadequacies are largely due to technical limitations, including the lack of methods for retrieving defective proteins in the soluble state. Indeed, the only available method for retrieving defective proteins has been the stepwise fractionation of protein aggregates by precise centrifugation (Koplin et al., 2010; Geladaki et al., 2019; Brennan et al., 2019), which is incompatible with retrieving phase-separated defective species, such as SG components (Koplin et al., 2010; Brennan et al., 2019). Less aggregation-prone defective proteins, such as IL-2Rα ΔSS (used as a model defective protein in Fig. 2) and CL1 (Fig. S2, A and B), and oligomeric inclusions occurring earlier in the aggregation process are also unlikely to be identified using centrifugation methods. Since TanGIBLE can trap target polypeptides before they aggregate, it provides a new avenue for profiling such a cryptic portion of endogenous defective (and hydrophobicity-exposed) proteins in the liquid phase in aneuploid cells. Indeed, TanGIBLE successfully retrieved a massive amount of endogenous polyubiquitinated species from the extracts of HeLa, a typical aneuploid human cell containing a total number of 76–90 chromosomes (Fig. 4 C).

It is interesting to note that HeLa cells contain more TanGIBLE-associated polyubiquitinated proteins compared with the cell line HCT116 (Fig. S3 F, top IP panel), even though the total amount of polyubiquitinated proteins in whole-cell lysates are comparable (or even less in HeLa cells) (Fig. S3 F, see middle input panel). The accumulation of hydrophobicity-exposed orphaned subunits might therefore be enhanced in HeLa cells. Whether these differences could be related to aneuploidy should be investigated in a future study.

Further engineering of TanGIBLE might improve its specificity and extend the range of its potential applications. For example, fusing other functional motifs, such as organelle targeting signals (e.g., nuclear or nucleolar targeting signals), to TanGIBLE might produce additional synergistic effects in a variety of spatiotemporal locations. Indeed, our preliminary experiments indicate that nuclear localization signal (NLS)-fused TanGIBLE co-immunoprecipitates polyubiquitinated entities robustly from a nuclear extract in a proteasome inhibition-dependent manner. Therefore, such modifications of TanGIBLE could expand the possible applications of this molecular probe, which would retain its specificity for exposed hydrophobic sites in defective proteins in specific organelles. Thus, further development of TanGIBLE derivatives will provide a novel method for understanding proteostasis occurring in, for example, nuclear protein quality control, viral antigen presentation, misregulated splicing, and genome aneuploidy.

In conclusion, this study presents a unique molecular device that preferentially targets defective polypeptides with exposed hydrophobicity. Comprehensive analysis of defective proteins using this probe will facilitate understanding the identity of aberrant proteomes generated by a wide variety of protein-misfolding diseases. Further improvements in the sensitivity and specificity of this designed protein and approaches for identifying defective proteins with exposed hydrophobicity in disease-associated cells are promising areas for future research.

Limitations of this tool

TanGIBLE can recognize a number of defective proteins with exposed hydrophobicity, but it cannot retrieve aberrant polypeptides lacking hydrophobic regions exposed to the cytosol or defective proteins enclosed by vesicular compartments. Although most proteasome subunits and ribosomal subunits were identified as TanGIBLE-associated proteins (see LC-MS/MS data in Table S1), we cannot distinguish at this moment whether these are retrieved as defective orphaned polypeptides or whether they are co-precipitated as an intact complex. We did not observe any apparent toxicity of TanGIBLE toward cell viability and proliferation but could not exclude the possibility of cryptic dominant negative effects of TanGIBLE, especially at higher expression levels.

Materials and methods

Plasmid construction

The cDNA of human BAG6 N200 was amplified by PCR. The PCR fragments were digested with *EcoRI* and *SalI* and inserted into

pCI-neo-based mammalian expression vectors (Promega). pCI-neo-3xFlag and pCI-neo-3xT7 expression vectors used in this study encode three repeats of Flag-tag (3xFlag) or T7-tag (3xT7) sequences, respectively, at the N-terminal or C-terminal regions of their products.

Six conserved hydrophobic residues in the BUILD domain (Met^{172}, Ile^{173}, Ile^{176}, Leu^{179}, Leu^{180}, and Met^{183} of human BAG6) were substituted with hydrophilic serine, and this substituent was designated as 6S mutant (Fig. 2 B).

Tandem-BAG6 N200 fragment (TanGIBLE) was constructed by PCR. The anterior cDNA encoding the first BAG6 N200 fragment was amplified without a termination codon at its 3′-end and cloned into pCI-neo-based mammalian expression vectors with restriction enzyme digestion of *XbaI* and *SalI*. The posterior cDNA encoding a second BAG6 N200 fragment was amplified by PCR with the sense primer encoding six repeats of glycine linker (Chichili et al., 2013) and with the antisense primer encoding stop codon and inserted into *SalI* and *NotI* site. Val and Glu residues in front of 6× Gly linker (sequence of VEGGGGGG) were derived from the *SalI* restriction enzyme site and regarded as a portion of the linker peptide. 10S TanGIBLE cDNA fragment was chemically synthesized by Eurofins Genomics and subcloned into pCI-neo-3xFlag and pCI-neo-3xT7 expression vectors.

Expression vectors encoding FL IL-2Rα and its truncated derivatives (ΔSS, ΔSSΔTMD, and ΔTMD), and CL1-fused luciferase were described in previous studies (Minami et al., 2010; Tanaka et al., 2016; Suzuki and Kawahara, 2016). Human insulin cDNA (originally purchased from Eurofins Genomics) with R6C mutation was prepared by PCR and subcloned into pCI-neo mammalian expression vector with C-terminal Flag- or T7-tags. Human prion cDNA (BC012844) encoding PrP with N3a- and Prl-type SS were chemically synthesized by Eurofins Genomics. All of the vectors used for experiments were verified by the sequencing of the inserted DNA.

Cell culture and transfection

HeLa cells (Bioresource Research Center [BRC] No# RCB0007; RIKEN BRC, Cat# CCL-2, RRID:CVCL_0030; ATCC) were cultured in Dulbecco's modified Eagle's medium (DMEM, Cat# 043-30085; Fuji-Wako Pure Chemical Industries, Ltd.) supplemented with 5% heat-inactivated fetal bovine serum (FBS, Cat# 10437028; Invitrogen,) at 37°C under 5% CO_2 atmosphere. HCT116 cells (BRC No#2979, RRID:CVCL_0291; RIKEN BRC) were cultured in DMEM with 10% FBS. All cell lines were authenticated by flow cytometry and were tested negative for mycoplasma contamination. Transfections of the expression vectors were performed with HilyMax (Cat# H357; Dojindo), HeLafect (OZ Biosciences), or polyethylenimine "MAX" transfection reagent (Cat# 24765-1; CAS 49553-93-7; Polysciences, Inc.) according to the protocol supplied by the manufacturer. At 24–48 h after transfection, the cells were harvested and subjected to immunological analysis.

Chemical treatments and heat stress

At 24–48 h after transfection of T7-tagged TanGIBLE or related fragments, the cells were subjected to treatments in the respective experiment as follows. For proteasome inhibition, HeLa cells were treated with 10 μM MG-132 (Cat# 3175-v; CAS 133407-82-6; Peptide Institute) or bortezomib (Cat# 021-18901; CAS 179324-69-7; Fujifilm-Wako) for 4 h as indicated. For the co-treatment of MG-132 and CHX (Cat# 033-20993; CAS 66-81-9; Fujifilm-Wako) in Fig. 4 D and Fig. S3 C, HeLa cells were treated with 25 μg/ml CHX and then 10 μM MG-132 for 4 h. After these chemical treatments, the cells were harvested and subjected to immunological analysis. For heat stress experiments in Fig. 4, A and B, TanGIBLE or its related fragments were expressed in HeLa cells, and cells were incubated at 44°C for 1 h in the absence of protease inhibitor. To induce the formation of stress granules, HeLa cells were treated with 5 μg/ml puromycin for indicated periods.

Immunological analysis

For immunoprecipitation analysis, HeLa cells were washed with ice-cold phosphate-buffered saline (PBS) and lysed with immunoprecipitation (IP) buffer containing 20 mM Tris-HCl pH 7.5, 150 mM NaCl, 5 mM EDTA, 1% Nonidet P-40, 10% Glycerol, and 25 μM MG-132. The lysates were sonicated for 5 s, centrifuged at 20,000 × *g* for 10–20 min at 4°C, and mixed with 5 μl of anti-Flag M2 affinity gel (A2220; Sigma-Aldrich; RRID: AB_10063035) or anti-T7 tag antibody agarose (69026; Merck Millipore; RRID: AB_10947861) for 10 min to 1 h at 4°C. After the beads had been washed at least three times with the IP buffer, the immunocomplexes were eluted with SDS sample buffer.

In the case of polyubiquitinated protein precipitations, 10 mM N-ethylmaleimide, 1 mM 4-(2-aminoethyl) benzenesulfonyl fluoride (AEBSF), 800 nM Aprotinin, 10 μM Pepstatin A, 15 μM E-64-d, and 20 μM Leupeptin were added to IP buffer. For the precipitation of polyubiquitinated proteins, 10 mM N-ethylmaleimide and 25 μM MG-132 should be included in the IP buffer during the entire procedure (including bead washing), probably due to co-precipitations of de-ubiquitinating enzyme(s) with the N-terminus of BAG6. The incubation with anti-Flag M2 affinity gel or anti-T7 tag antibody agarose was performed for 1 h at 4°C.

For western blot analyses, whole-cell lysates and the immunoprecipitates were subjected to SDS-PAGE with molecular weight marker (WIDE-VIEW Prestained Protein Size Marker III, Cat# 234-02464; Fujifilm-Wako) and transferred onto Immobilon-P transfer membrane (Cat# IPVH00010; Merck Millipore). The membranes were then immunoblotted with specific antibodies as indicated and then incubated with horseradish peroxidase–conjugated antibodies against mouse or rabbit immunoglobulins (Cat# NA931; RRID: AB_772210, Cat# NA934; RRID: AB_772206; GE Healthcare), followed by detection with ECL western blotting detection reagents (RPN2106; GE Healthcare), Clarity Western ECL substrate (Cat# 1705061; Bio-RAD). In the case of FK2 blot, blocking was performed by 3% bovine serum albumin in PBS containing 0.1% Tween 20, and the final detection was performed with Can Get Signal Immunoreaction Enhancer (Cat# NKB-101; CAS 9000-71-9; TOYOBO), in accordance with the manufacturer protocol.

The following antibodies were used in this study: anti-BAG6 rabbit polyclonal (Minami et al., 2010; RRID: AB_2934122), anti-polyubiquitin FK2 (RRID: AB_592937, RRID: AB_2934121; MBL or

Nippon Bio-Test Laboratories, Inc.), anti-puromycin (clone 12D10, MABE343, RRID:AB_2566826; Merck-Millipore), anti-PrP PRNP (D3Q5C) rabbit monoclonal (Cat# 14025; Cell Signaling Technology, RRID:AB_2798364), anti-basigin (Cat# 11989-1-AP; Proteintech, RRID:AB_2290597), anti-BST2 (Cat# 13560-1-AP; Proteintech, RRID:AB_2067220), anti-MCM2 (Cat# 10513-1-AP; Proteintech, RRID:AB_2142131), anti-MCM5 (Cat# 11703-1-AP; Proteintech, RRID:AB_2235162), anti-MCM6 (Cat# 13347-2-AP; Proteintech, RRID:AB_2142537), anti-MCM7 (Cat# 11225-1-AP; Proteintech, RRID:AB_2297584), anti-Flag M2 monoclonal (Cat# F3165; Sigma-Aldrich, RRID:AB_259529), anti-Flag polyclonal (Cat# F7425; Sigma-Aldrich, RRID:AB_439687), anti-T7-tag monoclonal (Cat# T8823; Sigma-Aldrich, RRID:AB_439708), and anti-α-tubulin (DM1A) monoclonal (Cat# T9026; Sigma-Aldrich, RRID:AB_477593).

Hot lysis analysis

HeLa cells were washed twice with PBS and lysed with hot lysis buffer containing 1% SDS, 50 mM Tris-HCl pH 7.5, 150 mM NaCl, 5 mM EDTA, 25 μM MG-132, 10 mM N-ethylmaleimide, and protease inhibitor cocktail. The lysates were heat-treated at 90°C for 15 min and sonicated. After the lysates were centrifuged at 20,630 × *g* for 20 min at room temperature, the supernatants were diluted fourfold with buffer A (containing 1% Triton-X100, 50 mM Tris-HCl pH 7.5, and 150 mM NaCl). Diluted extracts were mixed with 5 μl anti-Flag M2 affinity gel beads for 10 min at 4°C. After the beads had been washed five times with buffer A, the bounded immunocomplexes were eluted by SDS sample buffer and subsequently subjected to western blot analyses.

Immunoaffinity purification and trypsin digestion for the identification of TanGIBLE-associated proteins

We performed LC-MS/MS analyses using three independently prepared biological replicates. For direct immunoprecipitation of TanGIBLE-associated proteins, 4 × 10^6 harvested HeLa cells were washed with PBS and then lysed by sonication in IP buffer (20 mM Tris-HCl [pH 7.5], 5 mM EDTA, 150 mM NaCl, 10% glycerol, 25 μM MG-132, 10 mM N-ethylmaleimide [NEM], and 1% Nonidet P-40). Lysates were centrifuged at 20,000 × *g* for 15 min at 4°C. Protein concentration was estimated with the standard curve constructed for three different concentrations of BSA standards.

For 3xFLAG-tagged TanGIBLE or TR-TUBE immunoprecipitations, all steps were performed at 4°C unless otherwise noted. 0.5 ml of whole-cell lysates prepared from a 10-cm cell culture dish harvested 24 h after transfection was incubated with 15 μl of anti-FLAG M2 monoclonal antibody-conjugated agarose beads (Cat# A2220; Sigma-Aldrich, RRID:AB_10063035) for 1 h at 4°C. After the agarose beads were washed five times with 1.0 ml of IP buffer, bead-bound proteins were eluted for 2 h at 4°C with 500 μg/ml 3xFLAG-peptide (F4799; Sigma-Aldrich) buffered in PBS containing 25 μM MG-132 and 10 mM NEM. Proteins were reduced in 10 mM dithiothreitol for 10 min at 70°C and then alkylated with 15 mM iodoacetamide for 15 min at room temperature for on-beads tryptic digestion based on a single-pot solid-phase-enhanced sample preparation method using a KingFisher APEX (Thermo Fisher Scientific) (Müller et al., 2020). Alkylated proteins were incubated in 200 μl of 50% EtOH and conjugated with 40 μg of an equal mixture of hydrophobic and hydrophilic SeraMag SpeedBead carboxylate-modified magnetic particles (Cytiva), followed by desalting thrice with 400 μl of 80% EtOH. The magnetic beads were subjected to enzymatic digestion in 100 μl of 5 ng/μl Trypsin Gold (Promega) in 50 mM triethylammonium bicarbonate for 3.5 h at 37°C and rinsed out with 100 μl of pure water overnight at 37°C with 1 μg of trypsin (Promega). Digested peptides were acidified with 20 μl of 0.1% trifluoroacetic acid (TFA) and loaded into Evotip Pure (Evosep).

LC-MS/MS analysis

Desalted tryptic digests were analyzed by Evosep One (Evosep) coupled to an Orbitrap Fusion Lumos mass spectrometer (Thermo Fisher Scientific). Peptides were separated on a C18 analytical column (Aurora ELITE [1.7 μm, 75-μm i.d., and 15-cm length]; IonOpticks) using the defined 40SPD program. The Orbitrap Fusion Lumos mass spectrometer was operated in the data-dependent MS/MS mode with a mass range of 350–1,300 m/z and a resolution of 120,000 using Xcalibur software (RRID:SCR_014593; Thermo Xcalibur). The most intense ions (cycle time 3 s) were selected for MS/MS fragmentation with the higher-energy collisional dissociation (HCD) of 30, isolation window at 1.6 m/z, and maximum injection time at 22 ms in the centroid mode.

Protein identification from MS data

Proteome Discoverer software (version 3.1; RRID:SCR_014477; Thermo Fisher Scientific) was used to generate peak lists. The MS/MS spectra were searched against a UniProt Knowledgebase (*Homo sapiens* sp_canonical [TaxID = 9609] version 2023-09-13) using the Sequest HT search engine. The precursor and fragment mass tolerances were set to 10 ppm and 0.02 Da, respectively. Methionine oxidation, protein amino-terminal acetylation, and Gln/Asn deamidation were set as variable modifications, and Cys carbamidomethylation modification was set as a static modification for database searching. Peptide identification was filtered at a 1% false discovery rate. To identify specific targets of TanGIBLE, the results of three individual samples were assembled into one multiconsensus report using Proteome Discoverer software.

RNA interference

MCM2 and *MCM6* depletions in human cells were performed with duplex siRNAs covering the targeted sequences:

5′-UAUCAGAACUACCAGCGUATT-3′ (*MCM2* siRNA)
5′-ACCAUUCAAGAGGAGUUCUTT-3′ (*MCM6* siRNA).

As a negative control for siRNA experiments, AllStars Negative Control siRNA (Cat# 1027281; QIAGEN) was used unless otherwise noted. Transfections with duplex siRNA were performed using Lipofectamine RNAiMAX (Cat# 13778150; Thermo Fisher Scientific) according to the protocols provided by the manufacturer. The efficacy of each siRNA was verified by immunoblot with their specific antibodies.

Microscopic observations

For immunocytochemical observations, HeLa cells that were grown on a microcover glass (Matsunami) were washed

twice with ice-cold PBS, fixed by incubating in 4% paraformaldehyde for 30 min at 4°C, and permeabilized with 0.1% Triton X-100 for 3 min in room temperature. Fixed cells were blocked with 3% heat-inactivated calf serum in PBS and then reacted with a series of primary antibodies at 4°C for 16 h. Alexa Fluor 488-conjugated anti-rabbit IgG (Cat# A11001; Thermo Fisher Scientific Invitrogen; RRID: AB_2534069), and Alexa Fluor 594-conjugated anti-mouse IgG antibodies (Cat# A11037; Thermo Fisher Scientific Invitrogen; RRID: AB_2534095) were used as secondary antibodies at dilutions of 1:1,000. To observe the nucleus, cells were stained with Hoechst 33342. ProLong Glass Antifade Mountant Invitrogen was used as an imaging medium. Immunofluorescent images were obtained with BIOREVO BZ9000 fluorescence microscope (Keyence) or Nikon ECLIPSE Ti2-E with AX Confocal system with NIKON CFI super fluor 40× NA1.30 objective. NIKON 25 mm FOV galvano scanner, NIKON DUX-VB Detector, and NIS-Elements C-ER software were used for image acquisition. Adobe Photoshop (RRID:SCR_014199) was used for image processing.

For live cell detection of TanGIBLE, HeLa cells were grown in D-MEM high glucose without phenol red on the glass-bottom dish (Matsunami) and transfected with expression vectors encoding mCherry- or EGFP-fused TanGIBLE. 24 h after transfection, the dishes were observed with 30-min intervals at 37°C in a 5% CO_2 atmosphere using a NIKON Plan Apo 40× NA 0.95 objective lens with BIOREVO BZ9000 fluorescence microscope. Image J (RRID:SCR_003070) was used for movie production.

Preparation of the detergent-insoluble protein aggregate fraction

HeLa cells were treated with 10 μM MG-132 for 12 h and harvested with PBS containing 1% Triton X-100. The cell lysates were centrifuged at 20,000 × *g* for 20 min at 4°C, and the resulting precipitates were washed extensively with 1% Triton X-100 solution. The Triton X-100–insoluble protein aggregates were dissolved in SDS-PAGE sample buffer for western blot analysis.

Statistical analysis

Every experiment in this paper was repeated with at least three independent biological replicates to support the reproducibility of the results. Statistical analyses were performed using a Student's *t* test for two-sample comparisons. For multiple comparisons, statistical significance was tested by Dunnett's multiple comparisons test using the computing environment R version 3.5.1 (R Core Team 2022; https://www.r-project.org/). Data distribution was assumed to be normal but this was not formally tested. Statistical details of experiments are stated in the legends of figures displaying the respective data, including the statistical tests used and the number of replicates. All data in the figures are presented as the mean ± SD. P value of <0.05 is considered statistically significant.

Online supplemental material

Fig. S1 shows that TanGIBLE recognizes a mislocalized TMD protein more than N200. Fig. S2 shows TanGIBLE recognizes non-TMD model defective proteins. Fig. S3 shows that newly synthesized ubiquitinated proteins are endogenous clients of TanGIBLE. Fig. S4 shows LC-MS/MS–based identification of defective proteins trapped by TanGIBLE. Fig. S5 shows hydrophobic interactions between human MCM subunits. Fig. S6 shows TanGIBLE can visualize the cytoplasmic foci composed of defective proteins. Videos 1 and 2 show real-time detection of cytoplasmic foci in puromycin-treated cells. Table S1 is an Excel file for LC-MS/MS–based proteomics data.

Data availability

The mass spectrometry proteomics data have been deposited to the ProteomeXchange Consortium via the PRIDE partner repository with the dataset identifier PXD057470. Original data supporting the findings of this study are available from the corresponding author upon request.

Acknowledgments

We thank Dr. Ramanujan Hegde (MRC, Cambridge, UK) for providing us with plasmids encoding rodent versions of N3a-PrP and Prl-PrP. We also thank Dr. Yukiko Yoshida (IGAKUKEN, Tokyo, Japan) for providing us TR-TUBE expression vector. We thank Dr. Toshiki Takahashi, Dr. Aya Noguchi, Mr. Ryota Arai, Mr. Kazu Tajima, Mr. Takumi Hagiwara, Ms. Mayuri Yoshida, and Mr. Kei Wakita (Tokyo Metropolitan University) for their technical assistance. We are deeply grateful to the late Prof. Keiji Tanaka and Prof. Hideyoshi Yokosawa for their mentorship throughout our careers.

This work was supported in part by grants from the Japan Society for the Promotion of Science KAKENHI (Protein lifetime; No. 24H01905, No. 24K01978, No. 20H00457, Chemo-ubiquitin; No. 21H00289) to H. Kawahara. This work was also supported in part by the Takeda Science Foundation and Naito Foundation, Research Fund for Future Infectious Disease Measures and Advanced Research (R4-1) from the Tokyo Metropolitan Government to H. Kawahara. This study was partly supported by the Grant for International Joint Research Project of the Institute of Medical Science, the University of Tokyo.

Author contributions: Y. Iwasa: Conceptualization, Formal analysis, Investigation, Resources, Validation, Writing - original draft, S. Miyata: Conceptualization, Formal analysis, Investigation, Resources, Validation, Writing - original draft, T. Tomita: Investigation, Writing - review & editing, N. Yokota: Investigation, Methodology, Resources, M. Miyauchi: Formal analysis, Investigation, Validation, R. Mori: Formal analysis, Investigation, Validation, S. Matsushita: Investigation, Validation, R. Suzuki: Resources, Y. Saeki: Methodology, Resources, Supervision, Writing - review & editing, H. Kawahara: Conceptualization, Data curation, Funding acquisition, Methodology, Project administration, Resources, Supervision, Validation, Visualization, Writing - original draft, Writing - review & editing.

Disclosures: The authors declare no competing interests exist.

Submitted: 2 September 2021
Revised: 22 August 2024
Accepted: 26 November 2024

References

Akopian, D., and M. Rape. 2017. Conducting the finale of DNA replication. *Genes Dev.* 31:226–227. https://doi.org/10.1101/gad.297184.117

Arribere, J.A., E.S. Cenik, N. Jain, G.T. Hess, C.H. Lee, M.C. Bassik, and A.Z. Fire. 2016. Translation readthrough mitigation. *Nature.* 534:719–723. https://doi.org/10.1038/nature18308

Anderson, P., and N. Kedersha. 2002. Stressful initiations. *J. Cell Sci.* 115: 3227–3234. https://doi.org/10.1242/jcs.115.16.3227

Banerji, J., J. Sands, J.L. Strominger, and T. Spies. 1990. A gene pair from the human major histocompatibility complex encodes large proline-rich proteins with multiple repeated motifs and a single ubiquitin-like domain. *Proc. Natl. Acad. Sci. USA.* 87:2374–2378. https://doi.org/10.1073/pnas.87.6.2374

Ben-David, U., G. Arad, U. Weissbein, B. Mandefro, A. Maimon, T. Golan-Lev, K. Narwani, A.T. Clark, P.W. Andrews, N. Benvenisty, and J. Carlos Biancotti. 2014. Aneuploidy induces profound changes in gene expression, proliferation and tumorigenicity of human pluripotent stem cells. *Nat. Commun.* 5:4825. https://doi.org/10.1038/ncomms5825

Brennan, C.M., L.P. Vaites, J.N. Wells, S. Santaguida, J.A. Paulo, Z. Storchova, J.W. Harper, J.A. Marsh, and A. Amon. 2019. Protein aggregation mediates stoichiometry of protein complexes in aneuploid cells. *Genes Dev.* 33:1031–1047. https://doi.org/10.1101/gad.327494.119

Braunstein, I., L. Zach, S. Allan, K.U. Kalies, and A. Stanhill. 2015. Proteasomal degradation of preemptive quality control (pQC) substrates is mediated by an AIRAPL-p97 complex. *Mol. Biol. Cell.* 26:3719–3727. https://doi.org/10.1091/mbc.E15-02-0085

Chakrabarti, O., A. Ashok, and R.S. Hegde. 2009. Prion protein biosynthesis and its emerging role in neurodegeneration. *Trends Biochem. Sci.* 34: 287–295. https://doi.org/10.1016/j.tibs.2009.03.001

Chakrabarti, O., N.S. Rane, and R.S. Hegde. 2011. Cytosolic aggregates perturb the degradation of nontranslocated secretory and membrane proteins. *Mol. Biol. Cell.* 22:1625–1637. https://doi.org/10.1091/mbc.E10-07-0638

Ciechanover, A., and Y.T. Kwon. 2015. Degradation of misfolded proteins in neurodegenerative diseases: Therapeutic targets and strategies. *Exp. Mol. Med.* 47:e147. https://doi.org/10.1038/emm.2014.117

Chichili, V.P.R., V. Kumar, and J. Sivaraman. 2013. Linkers in the structural biology of protein-protein interactions. *Protein Sci.* 22:153–167. https://doi.org/10.1002/pro.2206

Chunduri, N.K., and Z. Storchová. 2019. The diverse consequences of aneuploidy. *Nat. Cell Biol.* 21:54–62. https://doi.org/10.1038/s41556-018-0243-8

Deegan, T.D., and J.F. Diffley. 2016. MCM: One ring to rule them all. *Curr. Opin. Struct. Biol.* 37:145–151. https://doi.org/10.1016/j.sbi.2016.01.014

Dephoure, N., S. Hwang, C. O'Sullivan, S.E. Dodgson, S.P. Gygi, A. Amon, and E.M. Torres. 2014. Quantitative proteomic analysis reveals posttranslational responses to aneuploidy in yeast. *Elife.* 3:e03023. https://doi.org/10.7554/eLife.03023

Duttler, S., S. Pechmann, and J. Frydman. 2013. Principles of cotranslational ubiquitination and quality control at the ribosome. *Mol. Cell.* 50: 379–393. https://doi.org/10.1016/j.molcel.2013.03.010

Edghill, E.L., S.E. Flanagan, A.M. Patch, C. Boustred, A. Parrish, B. Shields, M.H. Shepherd, K. Hussain, R.R. Kapoor, M. Malecki, et al. 2008. Insulin mutation screening in 1,044 patients with diabetes: Mutations in the INS gene are a common cause of neonatal diabetes but a rare cause of diabetes diagnosed in childhood or adulthood. *Diabetes.* 57:1034–1042. https://doi.org/10.2337/db07-1405

Escusa-Toret, S., W.I.M. Vonk, and J. Frydman. 2013. Spatial sequestration of misfolded proteins by a dynamic chaperone pathway enhances cellular fitness during stress. *Nat. Cell Biol.* 15:1231–1243. https://doi.org/10.1038/ncb2838

Fujimuro, M., H. Sawada, and H. Yokosawa. 1997. Dynamics of ubiquitin conjugation during heat-shock response revealed by using a monoclonal antibody specific to multi-ubiquitin chains. *Eur. J. Biochem.* 249: 427–433. https://doi.org/10.1111/j.1432-1033.1997.00427.x

Ge, X.Q., D.A. Jackson, and J.J. Blow. 2007. Dormant origins licensed by excess Mcm2-7 are required for human cells to survive replicative stress. *Genes Dev.* 21:3331–3341. https://doi.org/10.1101/gad.457807

Geladaki, A., N. Kočevar Britovšek, L.M. Breckels, T.S. Smith, O.L. Vennard, C.M. Mulvey, O.M. Crook, L. Gatto, and K.S. Lilley. 2019. Combining LOPIT with differential ultracentrifugation for high-resolution spatial proteomics. *Nat. Commun.* 10:331. https://doi.org/10.1038/s41467018-08191-w

Gilon, T., O. Chomsky, and R.G. Kulka. 1998. Degradation signals for ubiquitin system proteolysis in Saccharomyces cerevisiae. *EMBO J.* 17:2759–2766. https://doi.org/10.1093/emboj/17.10.2759

Goldberg, A.L. 2012. Development of proteasome inhibitors as research tools and cancer drugs. *J. Cell Biol.* 199:583–588. https://doi.org/10.1083/jcb.201210077

Guna, A., and R.S. Hegde. 2018. Transmembrane domain recognition during membrane protein biogenesis and quality control. *Curr. Biol.* 28: R498–R511. https://doi.org/10.1016/j.cub.2018.02.004

Guo, H., Y. Xiong, P. Witkowski, J. Cui, L.J. Wang, J. Sun, R. Lara-Lemus, L. Haataja, K. Hutchison, S.O. Shan, et al. 2014. Inefficient translocation of preproinsulin contributes to pancreatic β cell failure and late-onset diabetes. *J. Biol. Chem.* 289:16290–16302. https://doi.org/10.1074/jbc.M114.562355

Hessa, T., A. Sharma, M. Mariappan, H.D. Eshleman, E. Gutierrez, and R.S. Hegde. 2011. Protein targeting and degradation are coupled for elimination of mislocalized proteins. *Nature.* 475:394–397. https://doi.org/10.1038/nature10181

Hjerpe, R., F. Aillet, F. Lopitz-Otsoa, V. Lang, P. England, and M.S. Rodriguez. 2009. Efficient protection and isolation of ubiquitylated proteins using tandem ubiquitin-binding entities. *EMBO Rep.* 10:1250–1258. https://doi.org/10.1038/embor.2009.192

Huang, L., M.C. Kuhls, and L.C. Eisenlohr. 2011. Hydrophobicity as a driver of MHC class I antigen processing. *EMBO J.* 30:1634–1644. https://doi.org/10.1038/emboj.2011.62

Ibarra, A., E. Schwob, and J. Méndez. 2008. Excess MCM proteins protect human cells from replicative stress by licensing backup origins of replication. *Proc. Natl. Acad. Sci. USA.* 105:8956–8961. https://doi.org/10.1073/pnas.0803978105

Johnston, J.A., C.L. Ward, and R.R. Kopito. 1998. Aggresomes: A cellular response to misfolded proteins. *J. Cell Biol.* 143:1883–1898. https://doi.org/10.1083/jcb.143.7.1883

Juszkiewicz, S., and R.S. Hegde. 2018. Quality control of orphaned proteins. *Mol. Cell.* 71:443–457. https://doi.org/10.1016/j.molcel.2018.07.001

Kang, S.W., N.S. Rane, S.J. Kim, J.L. Garrison, J. Taunton, and R.S. Hegde. 2006. Substrate-specific translocational attenuation during ER stress defines a pre-emptive quality control pathway. *Cell.* 127:999–1013. https://doi.org/10.1016/j.cell.2006.10.032

Kawahara, H., R. Minami, and N. Yokota. 2013. BAG6/BAT3: Emerging roles in quality control for nascent polypeptides. *J. Biochem.* 153:147–160. https://doi.org/10.1093/jb/mvs149

Keenan, R.J., D.M. Freymann, R.M. Stroud, and P. Walter. 2001. The signal recognition particle. *Annu. Rev. Biochem.* 70:755–775. https://doi.org/10.1146/annurev.biochem.70.1.755

Kesner, J.S., Z. Chen, P. Shi, A.O. Aparicio, M.R. Murphy, Y. Guo, A. Trehan, J.E. Lipponen, Y. Recinos, N. Myeku, and X. Wu. 2023. Noncoding translation mitigation. *Nature.* 617:395–402. https://doi.org/10.1038/s41586-023-05946-4

Khan, S., R. de Giuli, G. Schmidtke, M. Bruns, M. Buchmeier, M. van den Broek, and M. Groettrup. 2001. Cutting edge: Neosynthesis is required for the presentation of a T cell epitope from a long-lived viral protein. *J. Immunol.* 167:4801–4804. https://doi.org/10.4049/jimmunol.167.9.4801

Kikukawa, Y., R. Minami, M. Shimada, M. Kobayashi, K. Tanaka, H. Yokosawa, and H. Kawahara. 2005. Unique proteasome subunit Xrpn10c is a specific receptor for the antiapoptotic ubiquitin-like protein Scythe. *FEBS J.* 272:6373–6386. https://doi.org/10.1111/j.1742-4658.2005.05032.x

Kim, S.J., D. Mitra, J.R. Salerno, and R.S. Hegde. 2002. Signal sequences control gating of the protein translocation channel in a substrate-specific manner. *Dev. Cell.* 2:207–217. https://doi.org/10.1016/s1534-5807(01)00120-4

Koplin, A., S. Preissler, Y. Ilina, M. Koch, A. Scior, M. Erhardt, and E. Deuerling. 2010. A dual function for chaperones SSB-RAC and the NAC nascent polypeptide-associated complex on ribosomes. *J. Cell Biol.* 189: 57–68. https://doi.org/10.1083/jcb.200910074

Kuwabara, N., R. Minami, N. Yokota, H. Matsumoto, T. Senda, H. Kawahara, and R. Kato. 2015. Structure of a BAG6 (Bcl-2-associated athanogene 6)-Ubl4a (ubiquitin-like protein 4a) complex reveals a novel binding interface that functions in tail-anchored protein biogenesis. *J. Biol. Chem.* 290:9387–9398. https://doi.org/10.1074/jbc.M114.631804

Lee, J.G., and Y. Ye. 2013. Bag6/Bat3/Scythe: A novel chaperone activity with diverse regulatory functions in protein biogenesis and degradation. *BioEssays.* 35:377–385. https://doi.org/10.1002/bies.201200159

Lelouard, H., E. Gatti, F. Cappello, O. Gresser, V. Camosseto, and P. Pierre. 2002. Transient aggregation of ubiquitinated proteins during dendritic cell maturation. *Nature.* 417:177–182. https://doi.org/10.1038/417177a

Lelouard, H., V. Ferrand, D. Marguet, J. Bania, V. Camosseto, A. David, E. Gatti, and P. Pierre. 2004. Dendritic cell aggresome-like induced

structures are dedicated areas for ubiquitination and storage of newly synthesized defective proteins. *J. Cell Biol.* 164:667–675. https://doi.org/10.1083/jcb.200312073

Levine, C.G., D. Mitra, A. Sharma, C.L. Smith, and R.S. Hegde. 2005. The efficiency of protein compartmentalization into the secretory pathway. *Mol. Biol. Cell.* 16:279–291. https://doi.org/10.1091/mbc.e04-06-0508

Li, N., Y. Zhai, Y. Zhang, W. Li, M. Yang, J. Lei, B.K. Tye, and N. Gao. 2015. Structure of the eukaryotic MCM complex at 3.8 Å. *Nature.* 524:186–191. https://doi.org/10.1038/nature14685

Liu, M., R. Lara-Lemus, S.O. Shan, J. Wright, L. Haataja, F. Barbetti, H. Guo, D. Larkin, and P. Arvan. 2012. Impaired cleavage of preproinsulin signal peptide linked to autosomal-dominant diabetes. *Diabetes.* 61:828–837. https://doi.org/10.2337/db11-0878

Ma, J., and S. Lindquist. 2001. Wild-type PrP and a mutant associated with prion disease are subject to retrograde transport and proteasome degradation. *Proc. Natl. Acad. Sci. USA.* 98:14955–14960. https://doi.org/10.1073/pnas.011578098

McShane, E., C. Sin, H. Zauber, J.N. Wells, N. Donnelly, X. Wang, J. Hou, W. Chen, Z. Storchová, J.A. Marsh, et al. 2016. Kinetic analysis of protein stability reveals age-dependent degradation. *Cell.* 167:803–815.e21. https://doi.org/10.1016/j.cell.2016.09.015

Meng, E.C., T.D. Goddard, E.F. Pettersen, G.S. Couch, Z.J. Pearson, J.H. Morris, and T.E. Ferrin. 2023. UCSF ChimeraX: Tools for structure building and analysis. *Protein Sci.* 32:e4792. https://doi.org/10.1002/pro.4792

Metzger, M.B., M.J. Maurer, B.M. Dancy, and S. Michaelis. 2008. Degradation of a cytosolic protein requires endoplasmic reticulum-associated degradation machinery. *J. Biol. Chem.* 283:32302–32316. https://doi.org/10.1074/jbc.M806424200

Minami, R., M. Shimada, H. Yokosawa, and H. Kawahara. 2007. Scythe regulates apoptosis through modulating ubiquitin-mediated proteolysis of the Xenopus elongation factor XEF1AO. *Biochem. J.* 405:495–501. https://doi.org/10.1042/BJ20061886

Minami, R., A. Hayakawa, H. Kagawa, Y. Yanagi, H. Yokosawa, and H. Kawahara. 2010. BAG-6 is essential for selective elimination of defective proteasomal substrates. *J. Cell Biol.* 190:637–650. https://doi.org/10.1083/jcb.200908092

Mock, J.Y., J.W. Chartron, M. Zaslaver, Y. Xu, Y. Ye, and W.M. Clemons Jr. 2015. Bag6 complex contains a minimal tail-anchor-targeting module and a mock BAG domain. *Proc. Natl. Acad. Sci. USA.* 112:106–111. https://doi.org/10.1073/pnas.1402745112

Mohsen, J.J., and S.A. Slavoff. 2023. Noncoding translation: Quality control in the BAG. *Mol. Cell.* 83:1967–1969. https://doi.org/10.1016/j.molcel.2023.05.033

Müller, M.B.D., P. Kasturi, G.G. Jayaraj, and F.U. Hartl. 2023. Mechanisms of readthrough mitigation reveal principles of GCN1-mediated translational quality control. *Cell.* 186:3227–3244.e20. https://doi.org/10.1016/j.cell.2023.05.035

Müller, T., M. Kalxdorf, R. Longuespée, D.N. Kazdal, A. Stenzinger, and J. Krijgsveld. 2020. Automated sample preparation with SP3 for low-input clinical proteomics. *Mol. Syst. Biol.* 16:e9111. https://doi.org/10.15252/msb.20199111

Muramatsu, T. 2016. Basigin (CD147), a multifunctional transmembrane glycoprotein with various binding partners. *J. Biochem.* 159:481–490. https://doi.org/10.1093/jb/mvv127

Oromendia, A.B., and A. Amon. 2014. Aneuploidy: Implications for protein homeostasis and disease. *Dis. Model. Mech.* 7:15–20. https://doi.org/10.1242/dmm.013391

Oromendia, A.B., S.E. Dodgson, and A. Amon. 2012. Aneuploidy causes proteotoxic stress in yeast. *Genes Dev.* 26:2696–2708. https://doi.org/10.1101/gad.207407.112

Parag, H.A., B. Raboy, and R.G. Kulka. 1987. Effect of heat shock on protein degradation in mammalian cells: Involvement of the ubiquitin system. *EMBO J.* 6:55–61. https://doi.org/10.1002/j.1460-2075.1987.tb04718.x

Payapilly, A., and S. High. 2014. BAG6 regulates the quality control of a polytopic ERAD substrate. *J. Cell Sci.* 127:2898–2909. https://doi.org/10.1242/jcs.145565

Polak, M., A. Dechaume, H. Cavé, R. Nimri, H. Crosnier, V. Sulmont, M. de Kerdanet, R. Scharfmann, Y. Lebenthal, P. Froguel, et al. 2008. Heterozygous missense mutations in the insulin gene are linked to permanent diabetes appearing in the neonatal period or in early infancy: A report from the French ND (neonatal diabetes) study group. *Diabetes.* 57:1115–1119. https://doi.org/10.2337/db07-1358

Qian, S.-B., M.F. Princiotta, J.R. Bennink, and J.W. Yewdell. 2006. Characterization of rapidly degraded polypeptides in mammalian cells reveals a novel layer of nascent protein quality control. *J. Biol. Chem.* 281:392–400. https://doi.org/10.1074/jbc.M509126200

Rajagopalan, H., and C. Lengauer. 2004. Aneuploidy and cancer. *Nature.* 432:338–341. https://doi.org/10.1038/nature03099

Rane, N.S., J.L. Yonkovich, and R.S. Hegde. 2004. Protection from cytosolic prion protein toxicity by modulation of protein translocation. *EMBO J.* 23:4550–4559. https://doi.org/10.1038/sj.emboj.7600462

Rane, N.S., S.W. Kang, O. Chakrabarti, L. Feigenbaum, and R.S. Hegde. 2008. Reduced translocation of nascent prion protein during ER stress contributes to neurodegeneration. *Dev. Cell.* 15:359–370. https://doi.org/10.1016/j.devcel.2008.06.015

Rane, N.S., O. Chakrabarti, L. Feigenbaum, and R.S. Hegde. 2010. Signal sequence insufficiency contributes to neurodegeneration caused by transmembrane prion protein. *J. Cell Biol.* 188:515–526. https://doi.org/10.1083/jcb.200911115

Reits, E.A., J.C. Vos, M. Grommé, and J. Neefjes. 2000. The major substrates for TAP in vivo are derived from newly synthesized proteins. *Nature.* 404:774–778. https://doi.org/10.1038/35008103

Rodrigo-Brenni, M.C., E. Gutierrez, and R.S. Hegde. 2014. Cytosolic quality control of mislocalized proteins requires RNF126 recruitment to Bag6. *Mol. Cell.* 55:227–237. https://doi.org/10.1016/j.molcel.2014.05.025

Ross, C.A., and M.A. Poirier. 2004. Protein aggregation and neurodegenerative disease. *Nat. Med.* 10:S10–S17. https://doi.org/10.1038/nm1066

Samant, R.S., V.B. Masto, and J. Frydman. 2019. Dosage compensation plans: Protein aggregation provides additional insurance against aneuploidy. *Genes Dev.* 33:1027–1030. https://doi.org/10.1101/gad.329383.119

Santaguida, S., E. Vasile, E. White, and A. Amon. 2015. Aneuploidy-induced cellular stresses limit autophagic degradation. *Genes Dev.* 29:2010–2021. https://doi.org/10.1101/gad.269118.115

Schubert, U., L.C. Antón, J. Gibbs, C.C. Norbury, J.W. Yewdell, and J.R. Bennink. 2000. Rapid degradation of a large fraction of newly synthesized proteins by proteasomes. *Nature.* 404:770–774. https://doi.org/10.1038/35008096

Skowera, A., R.J. Ellis, R. Varela-Calviño, S. Arif, G.C. Huang, C. Van-Krinks, A. Zaremba, C. Rackham, J.S. Allen, T.I. Tree, et al. 2008. CTLs are targeted to kill beta cells in patients with type 1 diabetes through recognition of a glucose-regulated preproinsulin epitope. *J. Clin. Invest.* 118:3390–3402. https://doi.org/10.1172/JCI35449

Stingele, S., G. Stoehr, K. Peplowska, J. Cox, M. Mann, and Z. Storchova. 2012. Global analysis of genome, transcriptome and proteome reveals the response to aneuploidy in human cells. *Mol. Syst. Biol.* 8:608. https://doi.org/10.1038/msb.2012.40

Støy, J., E.L. Edghill, S.E. Flanagan, H. Ye, V.P. Paz, A. Pluzhnikov, J.E. Below, M.G. Hayes, N.J. Cox, G.M. Lipkind, et al. 2007. Insulin gene mutations as a cause of permanent neonatal diabetes. *Proc. Natl. Acad. Sci. USA.* 104:15040–15044. https://doi.org/10.1073/pnas.0707291104

Suzuki, R., and H. Kawahara. 2016. UBQLN4 recognizes mislocalized transmembrane domain proteins and targets these to proteasomal degradation. *EMBO Rep.* 17:842–857. https://doi.org/10.15252/embr.201541402

Szeto, J., N.A. Kaniuk, V. Canadien, R. Nisman, N. Mizushima, T. Yoshimori, D.P. Bazett-Jones, and J.H. Brumell. 2006. ALIS are stress-induced protein storage compartments for substrates of the proteasome and autophagy. *Autophagy.* 2:189–199. https://doi.org/10.4161/auto.2731

Takahashi, T., S. Minami, Y. Tsuchiya, K. Tajima, N. Sakai, K. Suga, S.I. Hisanaga, N. Ohbayashi, M. Fukuda, and H. Kawahara. 2019. Cytoplasmic control of Rab family small GTPases through BAG6. *EMBO Rep.* 20:e46794. https://doi.org/10.15252/embr.201846794

Takahashi, T., J. Shirai, M. Matsuda, S. Nakanaga, S. Matsushita, K. Wakita, M. Hayashishita, R. Suzuki, A. Noguchi, N. Yokota, and H. Kawahara. 2023. Protein quality control machinery supports primary ciliogenesis by eliminating GDP-bound Rab8-family GTPases. *iScience.* 26:106652. https://doi.org/10.1016/j.isci.2023.106652

Tanaka, H., T. Takahashi, Y. Xie, R. Minami, Y. Yanagi, M. Hayashishita, R. Suzuki, N. Yokota, M. Shimada, T. Mizushima, et al. 2016. A conserved island of BAG6/Scythe is related to ubiquitin domains and participates in short hydrophobicity recognition. *FEBS J.* 283:662–677. https://doi.org/10.1111/febs.13618

Walter, P., and A.E. Johnson. 1994. Signal sequence recognition and protein targeting to the endoplasmic reticulum membrane. *Annu. Rev. Cell Biol.* 10:87–119. https://doi.org/10.1146/annurev.cb.10.110194.000511

Wang, Q., Y. Liu, N. Soetandyo, K. Baek, R. Hegde, and Y. Ye. 2011. A ubiquitin ligase-associated chaperone holdase maintains polypeptides in soluble states for proteasome degradation. *Mol. Cell.* 42:758–770. https://doi.org/10.1016/j.molcel.2011.05.010

Wang, F., L.A. Durfee, and J.M. Huibregtse. 2013. A cotranslational ubiquitination pathway for quality control of misfolded proteins. *Mol. Cell*. 50:368–378. https://doi.org/10.1016/j.molcel.2013.03.009

Wunderley, L., P. Leznicki, A. Payapilly, and S. High. 2014. SGTA regulates the cytosolic quality control of hydrophobic substrates. *J. Cell Sci.* 127: 4728–4739. https://doi.org/10.1242/jcs.155648

Xu, Y., Y. Liu, J.G. Lee, and Y. Ye. 2013. A ubiquitin-like domain recruits an oligomeric chaperone to a retrotranslocation complex in endoplasmic reticulum-associated degradation. *J. Biol. Chem.* 288:18068–18076. https://doi.org/10.1074/jbc.M112.449199

Yagita, Y., E. Zavodszky, S.Y. Peak-Chew, and R.S. Hegde. 2023. Mechanism of orphan subunit recognition during assembly quality control. *Cell*. 186:3443–3459.e24. https://doi.org/10.1016/j.cell.2023.06.016

Yamamoto, K., M. Hayashishita, S. Minami, K. Suzuki, T. Hagiwara, A. Noguchi, and H. Kawahara. 2017. Elimination of a signal sequence-uncleaved form of defective HLA protein through BAG6. *Sci. Rep.* 7: 14545. https://doi.org/10.1038/s41598-017-14975-9

Yewdell, J.W., E. Reits, and J. Neefjes. 2003. Making sense of mass destruction: Quantitating MHC class I antigen presentation. *Nat. Rev. Immunol.* 3:952–961. https://doi.org/10.1038/nri1250

Yewdell, J.W. 2011. DRiPs solidify: Progress in understanding endogenous MHC class I antigen processing. *Trends Immunol.* 32:548–558. https://doi.org/10.1016/j.it.2011.08.001

Yoshida, Y., Y. Saeki, A. Murakami, J. Kawawaki, H. Tsuchiya, H. Yoshihara, M. Shindo, and K. Tanaka. 2015. A comprehensive method for detecting ubiquitinated substrates using TR-TUBE. *Proc. Natl. Acad. Sci. USA*. 112: 4630–4635. https://doi.org/10.1073/pnas.1422313112

Zavodszky, E., S.Y. Peak-Chew, S. Juszkiewicz, A.J. Narvaez, and R.S. Hegde. 2021. Identification of a quality-control factor that monitors failures during proteasome assembly. *Science*. 373:998–1004. https://doi.org/10.1126/science.abc6500

Zhang, Z., B. Sie, A. Chang, Y. Leng, C. Nardone, R.T. Timms, and S.J. Elledge. 2023. Elucidation of E3 ubiquitin ligase specificity through proteome-wide internal degron mapping. *Mol. Cell*. 83:4191–4192. https://doi.org/10.1016/j.molcel.2023.10.021

JCB

Supplemental material

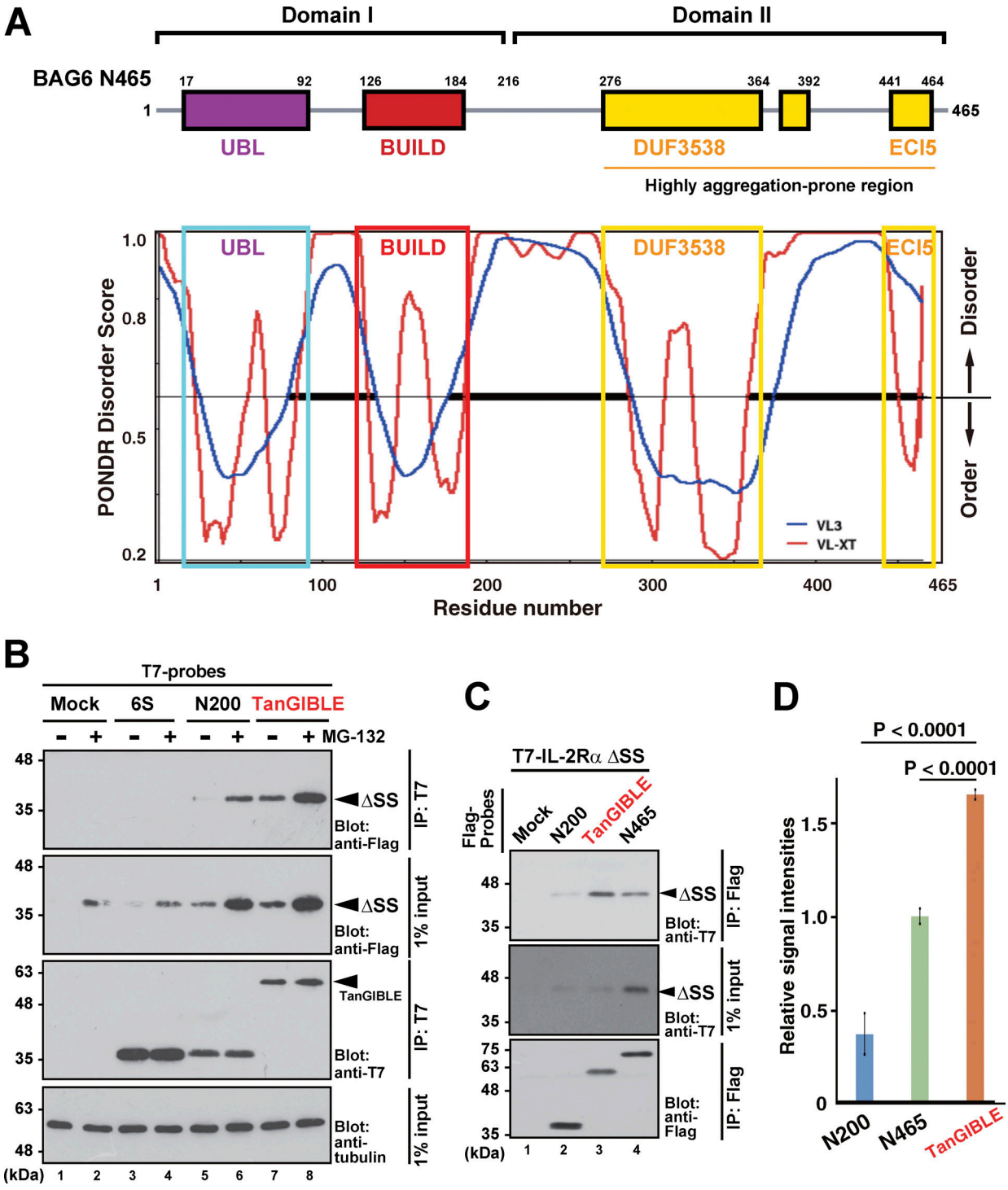

Figure S1. **TanGIBLE recognizes mislocalized TMD protein more than BAG6 N200 or N465 fragments. (A)** In relation to the Fig. 1, schematic of the domain structure of the N-terminal 465 residue region of human BAG6. Domain II contains DUF3538 (276–392, indicated by a yellow square). Low evolutionarily conserved sequences are indicated by gray lines. The amino acid sequence of BAG6 N465 was analyzed using PONDR. The stretches of the UBL sequence are indicated by blue boxes, the regions of the BUILD sequence are indicated by red boxes, and DUF3538 and other evolutionarily conserved regions in Domain II are indicated by yellow boxes. The results from two different predictor package, VL-XT (red line) and VL3 (blue line), are shown. **(B)** In relation to Fig. 2, improved detection of mislocalized IL-2Rα with TanGIBLE. T7-tagged BAG6 derivative fragments were immunoprecipitated (IP) and blotted using anti-Flag antibody to examine the interaction with Flag-IL-2Rα ΔSS. A N200-6S fragment (see Fig. 2 B) was used as the negative control. α-Tubulin was used as the loading control. **(C)** TanGIBLE co-precipitates more IL-2Rα ΔSS protein than BAG6 N200 and N465 fragments. After transfection with expression vectors encoding T7-IL-2Rα ΔSS and Flag-tagged BAG6 derivative fragments, anti-Flag immunoprecipitates were blotted with anti-T7 or anti-Flag antibodies. **(D)** Quantification of IL-2Rα ΔSS signals co-precipitated with Flag-tagged TanGIBLE. The graph represents the mean ± SD calculated from three independent biological replicates. P values were calculated using Dunnett's multiple comparisons test between N200, N465, and TanGIBLE. This statistical analysis was performed using the computing environment R version 3.5.1. Source data are available for this figure: SourceData FS1.

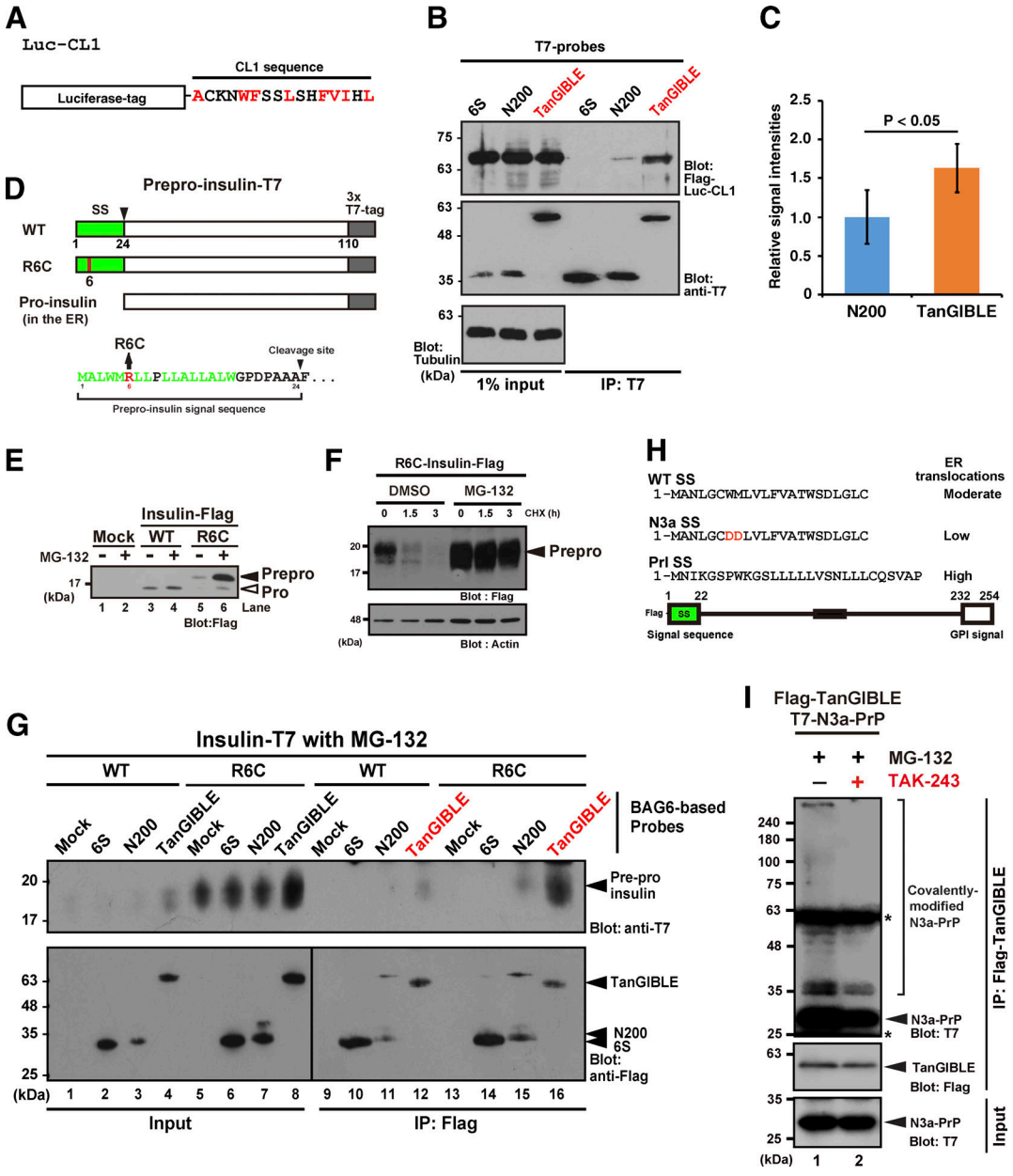

Figure S2. **TanGIBLE recognizes non-TMD model defective proteins. (A)** Schematic of the CL1-fused luciferase model defective protein used in this study. The CL1 degron sequence was fused at the C-terminus of luciferase (Luc) and the N-terminus of Luc was fused with three repeated Flag-tags. This artificial proteasomal substrate was designated as Flag-Luc-CL1. **(B)** TanGIBLE co-precipitates more CL1-fused luciferase than BAG6 N200. After the expression of Flag-Luc-CL1 and a series of T7-tagged probes, HeLa cells were treated with 5 μM MG-132 for 4.5 h. Anti-T7 precipitates were blotted using anti-FLAG or anti-T7 antibodies. α-Tubulin was used as a loading control. **(C)** Quantification of the relative signal intensity of Flag-Luc-CL1 co-immunoprecipitated (IP) with probes. The value of the co-precipitated Flag signal with N200 fragment was defined as a standard (as 1.0), and the relative value with TanGIBLE is indicated. The graph represents the mean ± SD calculated from eight independent biological replicates (n = 8). The P value was calculated using the Student's t test between N200 and TanGIBLE data. **(D)** Schematic representation of the mutations in the SS of prepro-insulin. A point mutation in the SS of R6C insulin was identified in pedigrees of type I diabetes (PNDM/MODY) with heterozygous mutations. SS are indicated in green. **(E)** An insulin R6C mutant accumulated as the prepro-form in proteasome-suppressed cells. HeLa cells expressing C-terminally Flag-tagged insulin WT or R6C were treated with (+) or without (–) 10 μM MG-132. At 4 h after MG-132 treatment, the cells were lysed and analyzed via immunoblotting using an anti-Flag antibody. **(F)** An insulin R6C mutant is unstable and degraded by the proteasome. HeLa cells expressing C-terminally Flag-tagged R6C insulin was chased with CHX in the presence or absence (DMSO) of 10 μM MG-132. The cells were lysed at the indicated time points and analyzed via immunoblotting using an anti-Flag-antibody. **(G)** TanGIBLE interacts with the ER-translocation-failed prepro-form of insulin mutants in proteasome-suppressed cells. HeLa cells expressing C-terminally T7-tagged insulin (WT or R6C) and Flag-tagged TanGIBLE were treated with 10 μM MG-132, as indicated. At 4 h after MG-132 treatment, the cells were lysed and immunoprecipitated with anti-Flag M2 agarose beads. Precipitates were blotted using the indicated antibodies. **(H)** Schematic representation of the human prion PrP and its SS mutants used in this study. Amino acid sequences of WT, N3a, and Prl (prolactin-type)-PrP SS are also provided. **(I)** Covalent modifications of N3a-PrP co-precipitated with TanGIBLE were weakened by the inhibition of ubiquitin-activating E1. MLN7243 was added to the cell cultures at 10 μM for 4 h before harvesting the cells (Takahashi et al., 2023). TanGIBLE immunoprecipitates from the cell lysates were probed with anti-T7 (PrP) antibody. The asterisk indicates the immunoglobulin signal. Source data are available for this figure: SourceData FS2.

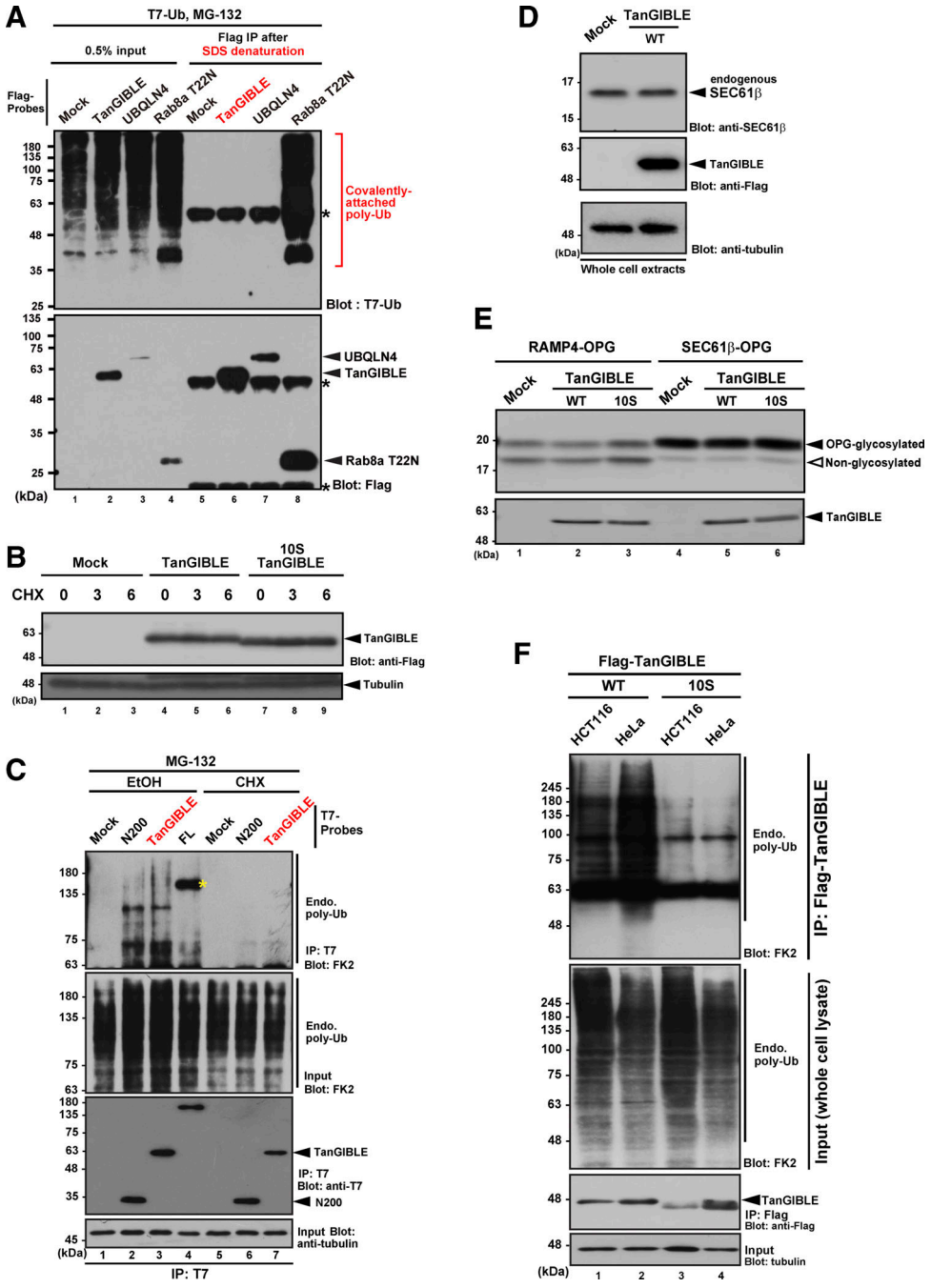

Figure S3. **Related to Fig. 4, newly synthesized ubiquitinated proteins are endogenous clients of TanGIBLE. (A)** Hot lysis immunoprecipitation (IP) analysis showed that SDS denatured TanGIBLE does not co-precipitate ubiquitin moieties. Flag-tagged TanGIBLE, UBQLN4, and Rab8a T22N mutant (a positive control for covalently polyubiquitinated protein) were expressed in MG-132–treated HeLa cells. The cell lysates treated with 1% SDS denaturation at 90°C were diluted with buffer A that did not include SDS, and then the samples were affinity-purified with anti-Flag antibody gel beads. Bounded proteins after precipitations were subjected to western blot analysis with anti-polyubiquitin FK2 or anti-Flag antibodies. Asterisk indicates signals of immunogloblin. **(B)** CHX-chase experiment suggested that both TanGIBLE and its 10S mutant are stable proteins in HeLa cells. Tubulin was used as a loading control. **(C)** Related to Fig. 4 D, polyubiquitinated proteins associated with TanGIBLE are sensitive to CHX. HeLa cells expressing T7-tagged TanGIBLE, BAG6 FL, or N200 fragments were treated with 25 μg/ml CHX (or its solvent, EtOH) and 10 μM MG-132 as indicated for 4 h, then affinity-purified with an anti-T7 antibody from cell extracts. T7-precipitates (IP:T7) were blotted with anti-polyubiquitin FK2 antibody to detect co-precipitated endogenous polyubiquitinated proteins. Yellow asterisks indicate signals of FL BAG6 cross-reacted with FK2 antibody. **(D and E)** TanGIBLE expression did not perturb the successful synthesis of tail-anchored proteins in HeLa cells. The expression level of endogenous SEC61β, a translocon subunit, was not affected by TanGIBLE expression (D). Two tail-anchored proteins, SEC61β and RAMP1, were C-terminally fused with opsin (OPG)-tag, a glycosylation site (E). Successful assembly of these tail-anchored proteins in the ER stimulates glycosyl modifications. These opsin-tagged tail-anchored proteins were co-expressed with TanGIBLE in HeLa cells. Glycosylations of these tail anchored proteins were not affected by TanGIBLE co-expression (E), suggesting that TanGIBLE does not perturb tail-anchored protein biogenesis. **(F)** TanGIBLE immunoprecipitates and their input extracts from HCT116 and HeLa cells were probed with FK2 anti-polyubiqitin antibody. Source data are available for this figure: SourceData FS3.

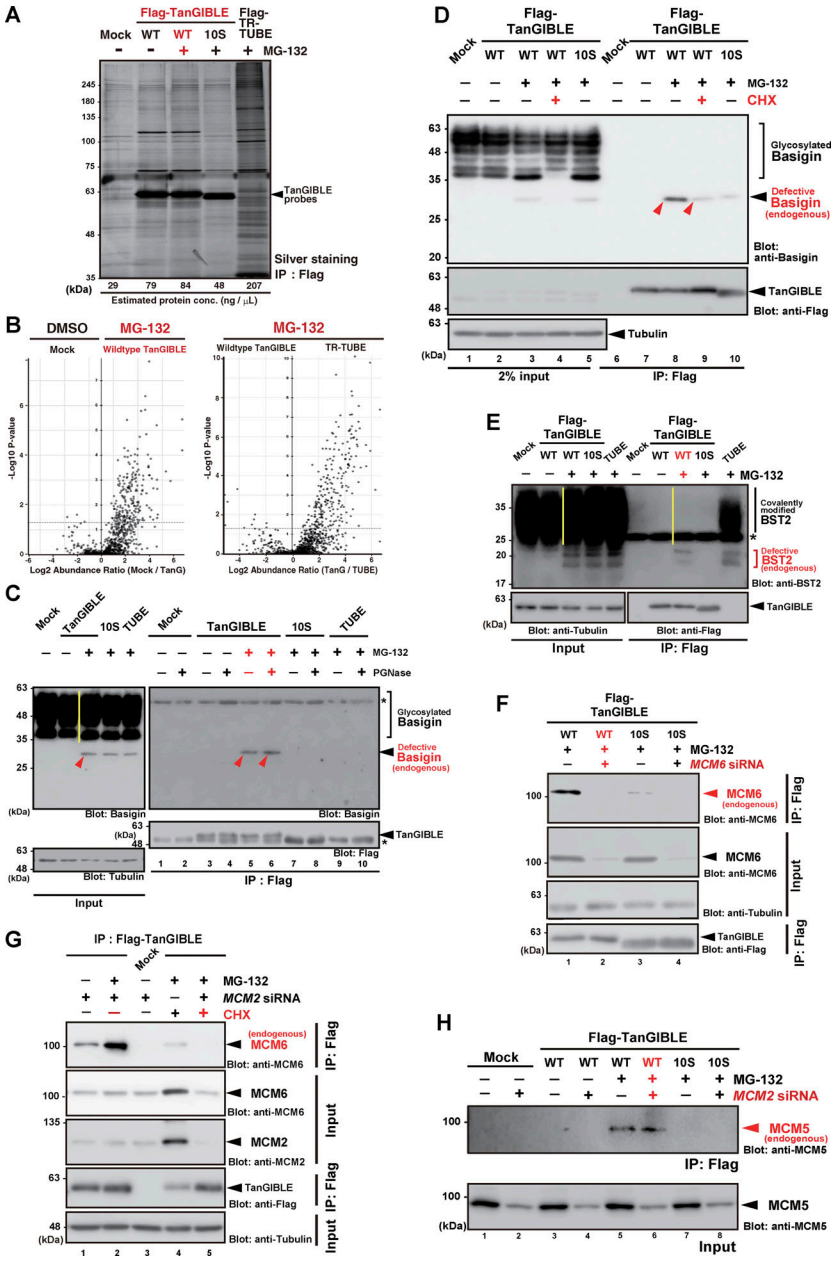

Figure S4. **Related to** Figs. 5 and 6**, LC-MS/MS–based identification of defective proteins trapped by TanGIBLE. (A)** Flag-TanGIBLE immunoprecipitates (IP) from MG-132–treated HeLa cell lysates were silver stained. Identical precipitates were anti-polyubiquitin immunoblotted in Fig. 5 A. The estimated protein concentration of each sample is noted at the bottom of the gel image. Note that Flag-TR-TUBE immunoprecipitated a much larger amount of protein, even though the protein expression level of Flag-TR-TUBE was below the limit of detection (Yoshida et al., 2015). **(B)** Immunoprecipitates shown in A were directly subjected to LC-MS/MS analysis. Volcano plot of TanGIBLE- or TR-TUBE–immunoprecipitates identified by deep MS analysis are shown. **(C)** TanGIBLE immunoprecipitates were treated with (+) or without (–) PGNase, a deglycosylation enzyme. Endogenous basigin in TanGIBLE precipitates (indicated by red arrowheads) was unaffected by deglycosylation treatment (compare lanes 5 and 6). Asterisk indicates signals of immunoglobulin. **(D)** TanGIBLE-associated basigin is sensitive to 4 h treatment with the protein synthesis inhibitor CHX. CHX was added to the cell culture 2 h prior to MG-132 addition. Defective basigins co-immunoprecipitated with TanGIBLE are indicated by red arrowheads. **(E)** Endogenous BST2 protein with no glycosyl modifications was co-immunoprecipitated with TanGIBLE. Note that successfully synthesized BST2 (indicated by a yellow line in the input lane) was not detected in the TanGIBLE precipitates (a yellow line in the IP lane). Note that TR-TUBE co-precipitated BST2 efficiently, supporting the observation that BST2 is a TUBE-preferred target protein (Fig. 5 F). Asterisk indicates a signal of immunoglobulin. **(F)** The MCM6 immunosignal that co-immunoprecipitated with TanGIBLE is specific since MCM6 siRNA canceled the corresponding signal in the TanGIBLE precipitates (compare lanes 1 and 2 in upper Flag IP panel). Tubulin is shown as a loading control for the input samples. **(G)** TanGIBLE-associated MCM6 is sensitive to protein synthesis inhibitor CHX. CHX was added to the cell culture 2 h prior to MG-132 addition. **(H)** Orphaned MCM5 subunit derived from disrupted MCM complex is a target of TanGIBLE. Although the total amount of MCM5 protein was greatly reduced by *MCM2* siRNA (lower input panel, compare lanes 5 and 6), endogenous MCM5 co-precipitated with TanGIBLE was not affected by MCM2 depletion (upper IP panel). Note that TanGIBLE-associated MCM5 is highly sensitive to 4 h MG-132 treatment. Anti-MCM7 immunoblot signals shown in Fig. 6 D were obtained by re-probing with identical membrane used in this figure. Note that molecular weights of MCM7 and MCM5 were different. Source data are available for this figure: SourceData FS4.

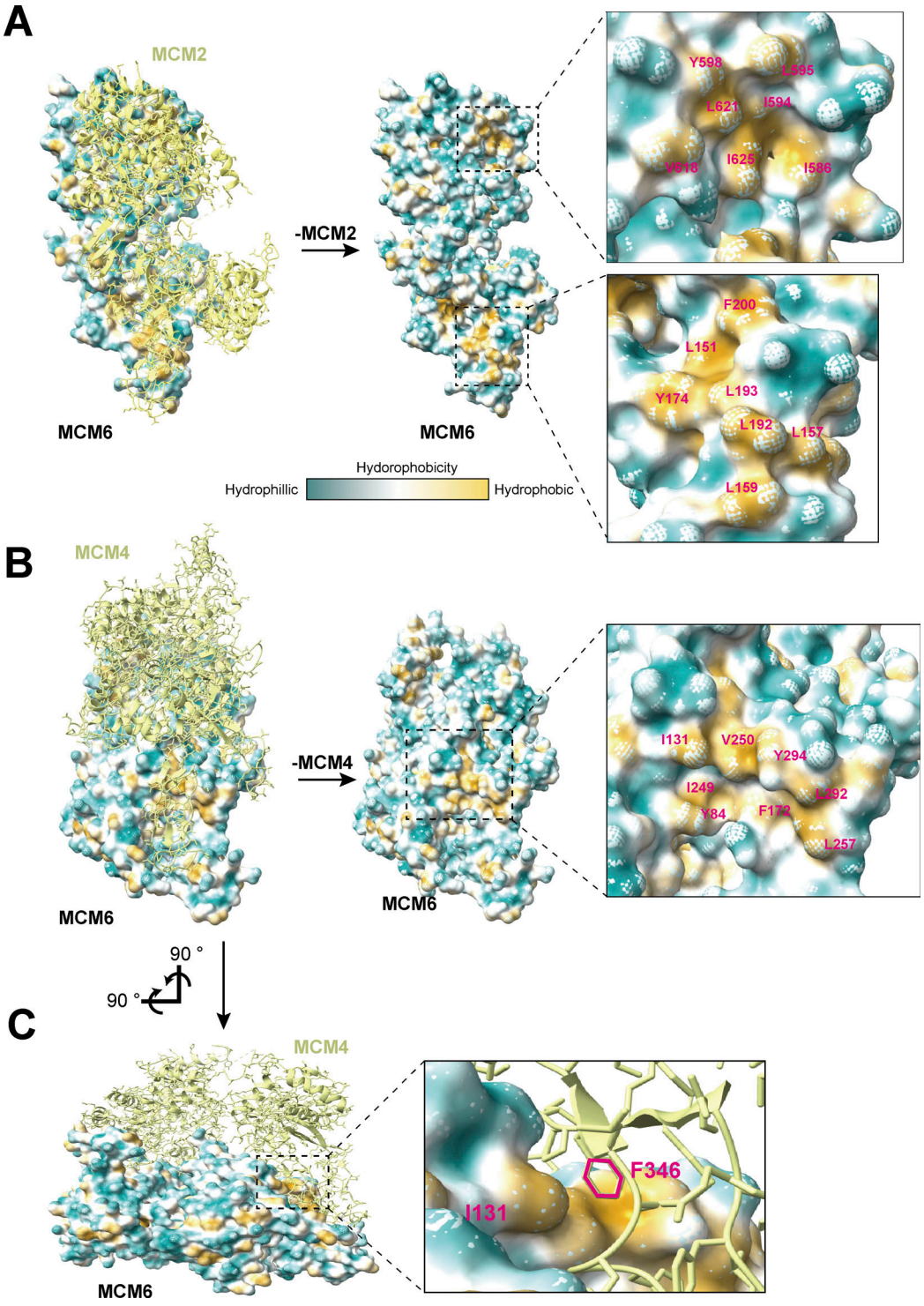

Figure S5. **Related to** Fig. 6**; hydrophobic interactions between human MCM subunits.** 6.77 Å resolution cryo-EM structure of the human MCM2/4/6 protein complex (PDB code 6XTY). Structural analyses were performed using ChimeraX (ver 1.8, https://www.cgl.ucsf.edu/chimerax/download.html) (Meng et al., 2023). **(A)** Interface between human MCM2 and MCM6 subunits. The structure of MCM2 is shown as a ribbon diagram and that of MCM6 is shown as a 3D density map with colored hydrophobicity surfaces. The zoomed view shows the hydrophobic patches on the surface of MCM6 that are covered by MCM2. **(B)** The interface between human MCM4 and MCM6 subunits. The structure of MCM4 is shown as a ribbon diagram and that of MCM6 as a 3D density map. The zoomed view shows the hydrophobic patches on the surface of MCM6 that are covered by MCM4. **(C)** Similar to the reported association between yeast MCM4 and MCM6, the hydrophobic interactions between Phe^{346} of human MCM4 and Ile^{131} of human MCM6 (which correspond to Phe^{391} of yeast MCM4 and Ile^{284} of yeast MCM6, respectively) are critical for driving this subunit–subunit interaction.

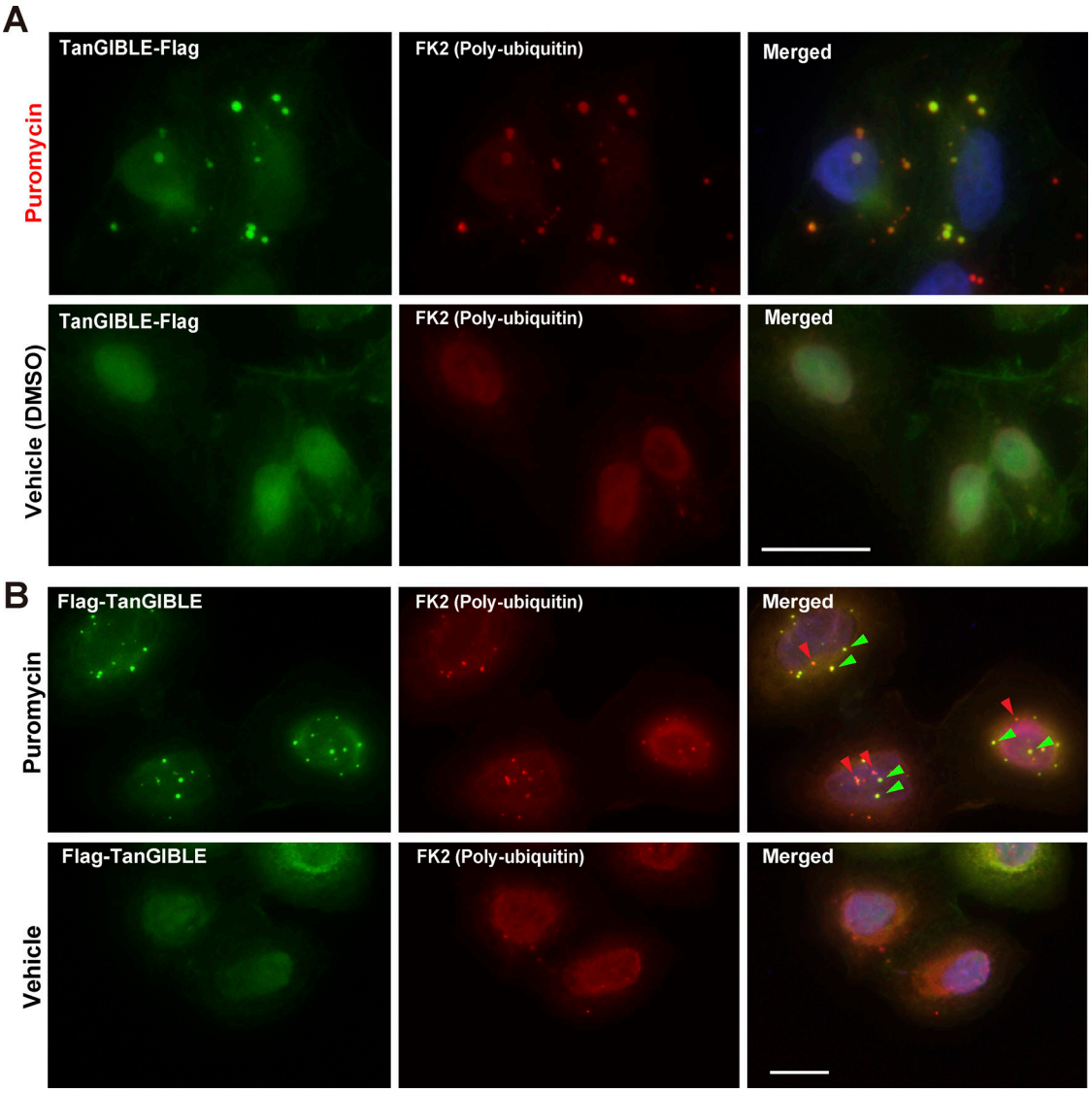

Figure S6. **TanGIBLE can visualize the cytoplasmic foci composed of defective proteins. (A and B)** In relation to Fig. 7, TanGIBLE can detect cytoplasmic foci composed of defective proteins. HeLa cells expressing C-terminally Flag-tagged TanGIBLE (A, TanGIBLE-Flag) or N-terminally Flag-tagged TanGIBLE (B, Flag-TanGIBLE) were treated with 10 µg/ml puromycin for 2 h, followed by 1% Triton X-100 extraction and 4% paraformaldehyde fixation. Fixed cells were stained with anti-Flag polyclonal (shown in green to detect TanGIBLE) and anti-polyubiquitin FK2 (shown in red to detect ubiquitin-positive cytoplasmic foci) antibodies. Note that signal intensities of TanGIBLE on respective foci do not correlate with those of polyubiquitin. For example, foci indicated with green arrowheads show far more intense TanGIBLE signals compared to polyubiquitin, while those with red arrowheads do not (B). TanGIBLE image was taken at 1/60 s exposure time, while polyubiquitin image was taken at 1/8 s, respectively. Scale bar: 20 µm.

Video 1. **Related to Fig. 7 B; real-time detection of cytoplasmic foci in puromycin-treated cells.** Live cell time-lapse detection of foci induced by puromycin treatment using fluorescent TanGIBLE. HeLa cells expressing EGFP-fused TanGIBLE were treated with 5 µg/ml puromycin, and fluorescence derived from TanGIBLE was monitored at 37°C in a 5% CO_2 environment using a Keyence fluorescence microscope BZ9000 (with 40× objective lens) for 300-min period with 30-min intervals. Playback speed is two frames per a second.

Video 2. **A negative control to Video 1.** Real-time detection of EGFP-10S TanGIBLE in puromycin-treated cells. Live cell detection of EGFP-fused 10S TanGIBLE under identical conditions to Video 1. HeLa cells expressing EGFP-fused 10S TanGIBLE were treated with 5 µg/ml puromycin, and fluorescence derived from 10S TanGIBLE was monitored at 37°C in a 5% CO_2 environment as Video 1. Playback speed is two frames per a second.

Provided online is Table S1. Table S1 shows LC-MS/MS–based proteomics data.